Embedded System Design and Joint Motion Control of a Quadruped Robot

by

Chonghan Ma

B. Eng., Hubei University of Technology, 2017

A Thesis Submitted in Partial Fulfillment of the

Requirements for the Degree of

MASTER OF APPLIED SCIENCE

in the Department of Mechanical Engineering

Embedded System Design and Joint Motion Control of a Quadruped Robot

by

Chonghan Ma

B. Eng., Hubei University of Technology, 2017

**Supervisory Committee**

---

Dr. Yang Shi, Supervisor

(Department of Mechanical Engineering)

---

Dr. Keivan Ahmadi, Departmental Member

(Department of Mechanical Engineering)

**Supervisory Committee**

---

Dr. Yang Shi, Supervisor

(Department of Mechanical Engineering)

---

Dr. Keivan Ahmadi, Departmental Member

(Department of Mechanical Engineering)

## Abstract

In recent decades, mobile robotics have become one of the fastest growing research fields. Compared with wheeled and tracked robots, legged robots can step over obstacles and traverse unstructured terrains. This thesis focuses on two main tasks for supporting the development of a quadruped robot, i.e., the robot embedded system design and the joint motion control.

To develop the robot embedded system fulfilling the technical requirements, a controller board using an ARM-based STM32 microcontroller is designed. First, we select the key components properly, according to the practical requirements and the marketing research. Then the onboard hardware architecture is proposed, and the circuit schematic diagrams for all the functional modules are designed. The specifications and a comparison of two versions of PCBs are also presented and analyzed.

Based on the designed embedded system, the actuators and sensors are tested, and selected to set up the robot experimental platform. Moreover, the firmware is configured, and the software is developed to control the position and velocity of

the motors. Furthermore, the moving average filter (MAF) based cascaded PID control algorithm is designed, and is implemented to manipulate the robot joints. The experimental results demonstrate the effectiveness of the proposed control method.

# Table of Contents

# List of Tables

# List of Figures

# Acronyms

| | |
|---|---|
| **DOF** | degree of freedom |
| **COG** | center of gravity |
| **CPU** | central processing unit |
| **PC** | personal computer |
| **CAN** | controller area network |
| **PAs** | proprioceptive actuators |
| **SEAs** | series elastic actuators |
| **BLDC** | brushless direct current |
| **IMU** | inertial measurement unit |
| **PID** | proportional-integral-derivative |
| **OS** | operation system |
| **CAD** | computer-aided design |
| **UART** | universal asynchronous receiver/transmitter |
| **USART** | universal synchronous/asynchronous receiver/transmitter |
| **RTOS** | real time operation system |
| **RAM** | random access memory |
| **ROM** | read only memory |
| **FPU** | floating point unit |
| **SWD** | serial wire debug |
| **I/O** | input/output |
| **MCU** | microprogrammed control unit |
| **SPI** | serial peripheral interface |
| **DC/DC** | direct current to direct current |
| **AC/DC** | alternating current to direct current |
| **LDO** | low-dropout |
| **IC** | integrated circuit |
| **PWM** | pulse-width modulation |
| **PCB** | printed circuit board |
| **MOSFET** | metal–oxide–semiconductor field-effect transistor |
| **A/D** | analog to digital |
| **MAF** | moving average filter |
| **IDE** | integrated development environment |
| **FPGA** | field-programmable gate array |

# Acknowledgements

Firstly, I would like to express my sincere gratitude to my supervisor, Dr. Yang Shi for providing me with the precious opportunity to work in such an amazing field during my MASc study at UVic. His immense knowledge and insightful suggestions always inspire me to move forward. He not only encouraged me with great patience to promote my academic abilities, but also provided tons of experience on becoming a responsible and mature person. I have gained an invaluable amount of knowledge and experience working under his supervision.

I wish to thank the thesis committee members, Dr. xxx and Dr. xxx, for their constructive suggestions.

Moreover, I am also thankful to all my labmates from Applied Control and Information Processing Lab (ACIPL), it is my honor to work with you all. In particular, I am grateful to Dr. Bingxian Mu for picking me up when I arrived in Victoria, to Xiang Sheng for providing kindness help on the project. I would also like to thank Dr. Chao Shen, Dr. Yuanye Chen, Jicheng Chen, Kunwu Zhang, Yuan Yang, Qi Sun, Qiao Zhang, Changxin Liu, Henglai Wei, Tianyu Tan, Xinxin Shang, Zhang Zhang, Chen Ma, Huaiyuan Sheng, Zhuo Li, and Tianxiang Lu for the impressive time we spent together. Thanks also go to my reliable friends Dr. Chunxi Yang, Dr. Liying Hao, Dr. Fengqiu Xu, Kenan Yong, Hongwei Sun, Xin Jin, Shichang Cui, Chengsi Shang, Chenglong Du, Meng Li, Dong Wang and Lu Ren for their selfless help.

Finally, I would like to thank my parents for their never-ending love, support and encouragement during this whole journey.

To my parents

To my grandfather

# Chapter 1

# Introduction

## 1.1 An Overview on Mobile Robots

Autonomous robots can be roughly classified into two categories, stationary robots and mobile robots. One type of stationary robotic systems is the manipulator, which places surface-mounted components with extremely high precision [1], i.e., in the assembly line, a robot arm is able to move with high speed and accuracy to perform repetitive tasks, such as spot welding [2] and painting [3]. Another important type of stationary robotic systems is the grasping device [4], which is commonly used to grasp the desired objects. Nowadays, a variety of robotic hand and finger mechanics have been developed and have been widely applied in agriculture [5], etc. Unfortunately, these stationary robots are suffering from the lack of mobility and limited range of motion.

In contrast, mobile robots are able to move over rough terrains. Due to flexibility of the mobile robots, they are widely applied in many areas such as planetary exploration, medical care, and construction, etc. In these application scenarios, mobile robots can be classified into land-based robots, aerial robots, and underwater robots.

Furthermore, according to different mechanical structures, the land-based robots can be divided into wheeled robots, tracked robots, and legged robots, respectively.

### 1.1.1 Wheeled and Tracked Robots

As one of the most important systems for robot locomotion, wheeled robots play significant roles in transportation [6] and logistics [7]. Generally, wheeled robots move faster and consume less energy than tracked vehicles. Meanwhile, they also tend to be much cheaper and do not present difficulties in terms of balance issues, in comparison with their legged counterparts. Therefore, the control strategies for wheeled robots are less complex than other solutions. Compared to conventional wheeled robots, tracked robots feature larger ground contact patches and less ground impact [8]. However, they are less precise in maneuverability and more difficult to get repaired.

### 1.1.2 Legged Robots

In nature, there are some specific places, such as planetary surfaces [9, 10, 11], construction [12, 13], and disaster salvation [14, 15], etc. These circumstances are mostly uneven terrains, which limit the application of wheeled robots and tracked robots. However, legged robots are more suitable in these situations for locomotion implementation, by virtue of their terrain adaptation ability. In addition, they can also be applied in plenty of fields, such as medical applications [16, 17] and education [18]. Therefore, the legged robot has become a hot spot in robotics research, due to their advantages over wheeled and tracked robots.

Firstly, legged robots present superior mobility in natural terrains. Unlike wheeled robots, they can avoid small obstacles by making discrete footholds without the necessity of continuous support surface. Moreover, the use of multiple degrees of freedom

(DOFs) in the leg joints adjusts the leg extension to position the center of gravity (COG) of the body, and further varies the body height. Hence, legged robots are able to move over irregular terrains by adjusting their leg configurations.

The other advantage is that legged robots have redundant legs, and therefore they can maintain balance and continue walking even with one leg mutilated during static locomotion, which improves failure tolerance [19, 20]. Additionally, the legs can work as an active support base to flexibly actuate the robot body when feet are fixed to the ground [21].

Although legged locomotion is advantageous compared with traditional wheeled and tracked vehicles, legged robots also have drawbacks. They require complex mechanical design and control algorithm. Furthermore, they are heavier and consume larger energy since a large number of actuators are required to manipulate multiple DOFs legs. There are many types of walking robots depending on the number of legs.

- ***Monopod***

The Monopod robots have only one type of locomotion gait, i.e., hopping, which represents a highly nonlinear dynamical behavior, consisting of alternating flight and stance phases. As shown in Figure 1.1(a), a Toyota monopod robot [22] developed by *Tajima* and *Suga* in 2006 has a total of seven DOFs, three at the hip, one at the knee, two at the ankle, and one at the toe, with one extra DOF for 3D motion. This redundancy is beneficial for reducing the excessive joint speed when it is hopping. Another distinctive jumping robot, named as Salto-1p [23, 24], was created by UC Berkeley's Biomimetic Millisystems Lab in 2017. It is designed to mimic saltatorial animals like galago or bushbaby, which has a strong vertical jumping agility, as shown in Figure 1.1(b).

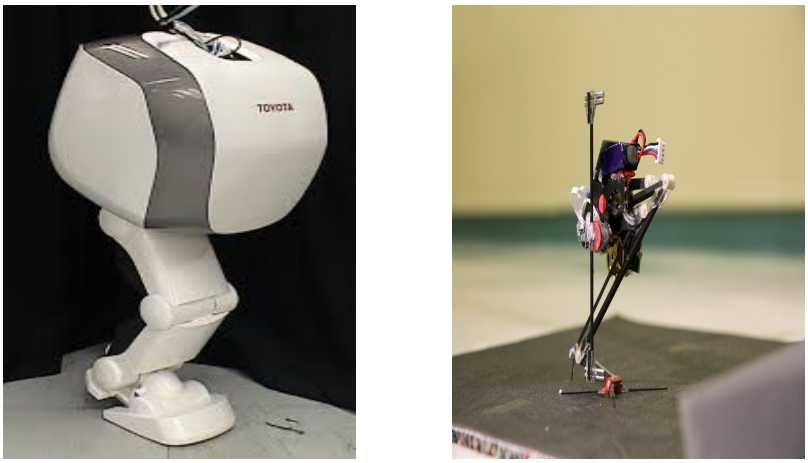


(a) (b)

Figure 1.1: (a) "Toyota monopod" [22] and (b) "Salto-1P" [23, 24].

- ***Bipedal robot***

Bipedal robots make use of sensors to reproduce human capabilities, such as going up and down stairs, jumping, or even doing somersaults. As illustrated in Figure 1.2(a), the biped "REEM-C" is a 100% ROS-based bipedal robotics platform, which was launched by PAL Robotics in 2013 [25]. It is controlled by two computers with Intel Core i7-2710QE CPUs. The sonars and cameras help to map its environment, perform path planning, and achieve obstacle avoidance. The MTi-30 AHRS sensor provides the real-time attitude information and improves walking stability. In addition, all the motors and sensors communicate with the PC via CAN network. In 2017, a new humanoid robot "TALOS" [26], also launched by PAL Robotics, is mainly used for artificial intelligence and human-robot interaction, as shown in Figure 1.2(b). It is a fully electrical actuated and torque-controllable robot, assembled with torque sensors and EtherCAT communication network to manipulate up to 6 kg payload for each stretched arm.

(a)

(b)

Figure 1.2: (a) "REEM-C" [25] and (b) "TALOS" [26].

- ***Quadruped robot***

Quadruped robots have the advantage of being statically stable when they are not moving. However, dynamic walking control for leg coordination becomes more complicated and high computational speed is required. Moreover, according to different types of actuators, the application scenarios and control performance are different. As shown in Figure 1.3(a), the "HyQReal" is developed to support humans in emergency scenarios, presented by IIT (Istituto Italiano di Tecnologia) in 2019 [27]. It is an electro-hydraulic powered quadruped robot that features high ruggedness, reliability and energy efficiency. Combined with large output driving force, fast response speed of the hydraulic actuator and compact structure of the electric motors, it can pull a small passenger airplane weighing more than 3 tons. Additionally, it is controlled by two computers on board: One is dedicated to vision and the other is for control.

As pictured in Figure 1.3(b), the "Cheetah 3" is designed to move across rough terrain and through obstacles without relying on vision, built by MIT in 2018 [28]. It is driven by self-made proprioceptive actuators (PAs), which have high torque density to improve the load-carrying ability and low-speed efficiency. The actuation

system is designed to achieve certain tasks, such as power plant inspection and blind locomotion, which makes the robot suited for reconnaissance and rescue missions. The locomotion control and state estimation are handled by an embedded computer with a second GEN Core i7 CPU, while the leg controller is performed by an ARM-A8 processor.

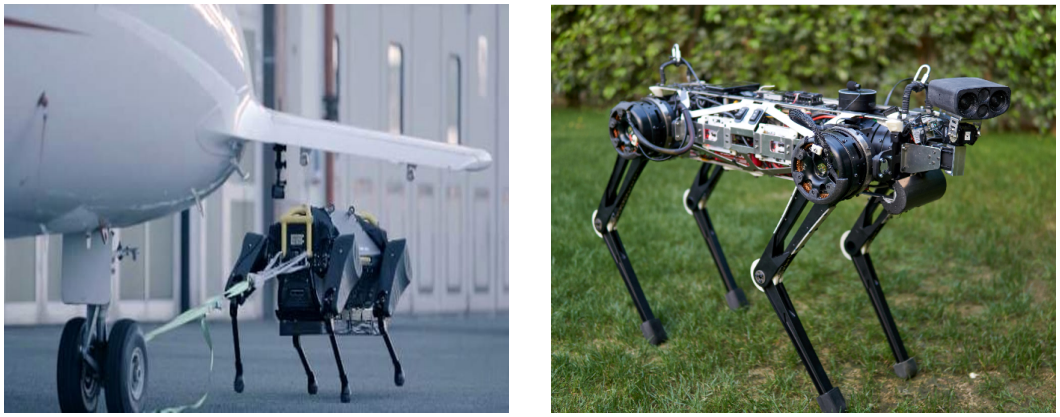

(a) (b)

Figure 1.3: (a) "HyQReal" [27] and (b) "Cheetah 3" [28].

Laikago [29], released by Unitree Robotics in 2017, is a lightweight quadruped robot research platform and actuated by 12 Unitree brushless DC motors, as shown in Figure 1.4(a). It is capable to maintain stability as the terrain changes and adjust the posture automatically. Therefore, Laikago is applied to perform tasks such as security patrolling, deliveries or research studies.

ANYmal is designed for autonomous operation in challenging environments, created by ETH Zurich and ANYbotics in 2016 [30]. Driven by special compliant and highly integrated series elastic actuators (SEAs), the robot is capable of wide range of motion and high-mobile climbing. The robot navigation is achieved by using onboard thermal cameras, microphones and Lidar scanners. Furthermore, it can open doors autonomously, walk upstairs in any terrain, and crawl through tight spaces by changing the leg configurations.

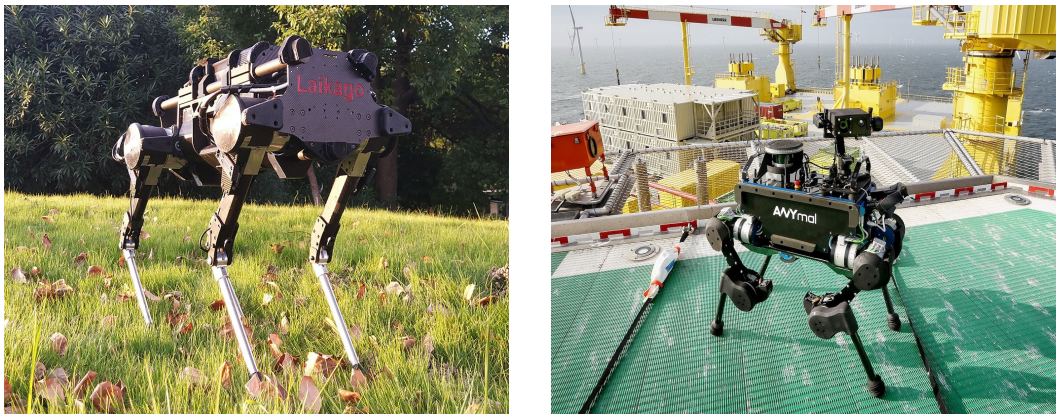


(a) (b)

Figure 1.4: (a) "Laikago" [29] and (b) "ANYmal" [30].

The performance of mobile robots can be further improved by using different locomotion modes, and thus hybrid locomotion robots have been studied and developed in recent years [31, 32, 33]. This type of robot structure takes the advantages of various locomotion modes and switches between different modes according to the practical requirements and terrain conditions.

## 1.2 Robot Control System

Essentially, an industrial robot control system consists of three elements: Actuator, sensor and the embedded system. The actuators are used to produce mechanical movements in robots or tell what the robot is doing. Moreover, the sensors measure the physical properties of the surrounding environment to increase the performance of robot to a large extent. More importantly, the embedded system globally interconnects every subsystem and performs different tasks simultaneously. Thus, the embedded system is the centerpiece of a robot control system.

### 1.2.1 Actuators

There are three types of actuators (electric, hydraulic and pneumatic) which are most commonly used to actuate the robot joints.

Electric robots are usually driven by permanent magnet servo motors, brushless motors and stepper motors. Compared with fluid power machines, electric actuation systems are easily maintained and are suitable for electronic control. However, unless incorporating direct-drive motors, electrically driven robots have the limitation of requiring transmission systems. It can not only add cost and weight, but also reduce precision and efficiency due to gear backlash or undesired friction. Furthermore, if their maximum permitted torque is exceeded, the gears are increasingly becoming the weakest element of an electric motor unit [34] with the risk of breaking. Additionally, electric motors produce low torque relative to their size and weight.

Hydraulically powered robots have very good power-to-weight ratio and hydraulic force can be applied directly at the desired point without the necessity of a transmission system. In addition, there are no backlash problems, as hydraulic fluid is incompressible. Because of the sturdy construction, they can withstand higher shock loads than other robot types. However, they tend to be less reliable than electric robots due to fluid leaks which contaminates the work areas and causes performance loss. Moreover, hydraulic robots tend to be much more expensive than their electric counterparts.

Pneumatic powered robots are the cheapest and least sophisticated type. They are fast, reliable and easily understood by technicians. Meanwhile, they can also be used to detect gas leakage [35]. The major weakness of the pneumatic robots is that precise servo control is not practical due to compressibility of the air, particularly when moving heavier loads. Thus, pneumatic robots are usually found in light-load and fixed-speed applications. The most important properties of the electric, pneumatic

and hydraulic actuators are listed in Table 1.1.

Table 1.1: Comparison of three conventional actuator types [36].

| Property | Electric | Hydraulic | Pneumatic |
|---|---|---|---|
| Working principle | electricity | high quality oil, synthetic liquids | air, nitrogen, combustion |
| Power supply | ≤460V | 0.4-70MPa | 0.04-0.9MPa |
| Efficiency | high | low | low |
| Speed | fast | relatively fast | slow |
| Position accuracy | high | good | good |
| Energy consumption | low | high | high |
| Power-to-weight ratio | low | high | relatively high |
| Noise | low | relatively high | relatively high |
| Temperature sensitivity | insensitive | sensitive | relatively sensitive |
| Cost | relatively low | high | low |

### 1.2.2 Sensors

It is vital for an autonomous mobile robot to acquire knowledge about its work environment. This can be achieved by collecting data via sensors. For instance, the use of sensors makes it possible to perform robot positioning and localization tasks [37]. In addition, they are widely used for mapping [38] and object recognition [39]. Generally, the sensors can be grouped into internal and external sensors. Internal sensors are utilized to measure the parameters of the robot itself, such as the motor speed, joint angle, etc. External sensors obtain surrounding information, such as the distance, light intensity, and sound amplitude. The most common sensors used in the robot control systems are as follows:

- ***Potentiometers*** are a type of resistive transducers and the output voltage is proportional to the displacement. They are primarily used to measure the angular position in the robot control systems, with feedback loops to ensure that the joints reach the desired positions.

- ***Force and torque sensors*** are always mounted in each leg of the robot. They can detect the ground contact angle and measure the amount of force between the foot and ground, and further adjust the robot posture.

- ***Encoders*** measure the position and speed of the motors, i.e., a rotary shaft encoder uses a disk which is read by an optical photodetector inside the encoder to output the digital signal that indicates the angular position of the shaft.

- ***IMUs*** usually contain accelerometers and gyroscopes. Accelerometers measure the acceleration, from which velocity can be obtained by integration. In most cases, IMU is used to measure angular velocities and orientation.

- ***Laser range finder*** uses a laser beam to generate highly precise distance measurements. The distance between sensor and target is measured by calculating the speed of light and the time it takes for emitted light to return to the receiver.

- ***Vision-based sensors*** process data from any modality and use the electromagnetic spectrum to produce images. The two current technologies for devising vision sensors are CCD and CMOS [40].

- ***Depth sensors*** are used in object detection, scene reconstruction, 3D inspection, and so on. Two elements must always be present in a depth sensor: An infrared (IR) projector and an IR camera.

### 1.2.3 Embedded System

Embedded system is a scaled down computer, which is designed to perform specific tasks. Compared with a computer platform, embedded system is much easier to design, less expensive and more portable, therefore, it is widely used in the mobile robot applications. The embedded system interfaces with the robot internal and external sensors, actuators, and other peripheral components. Thus, it is capable to handle serial and parallel data transmission at various rates, and carry out A/D and D/A conversion. The flow diagram of an overall embedded system is illustrated in Figure 1.5.

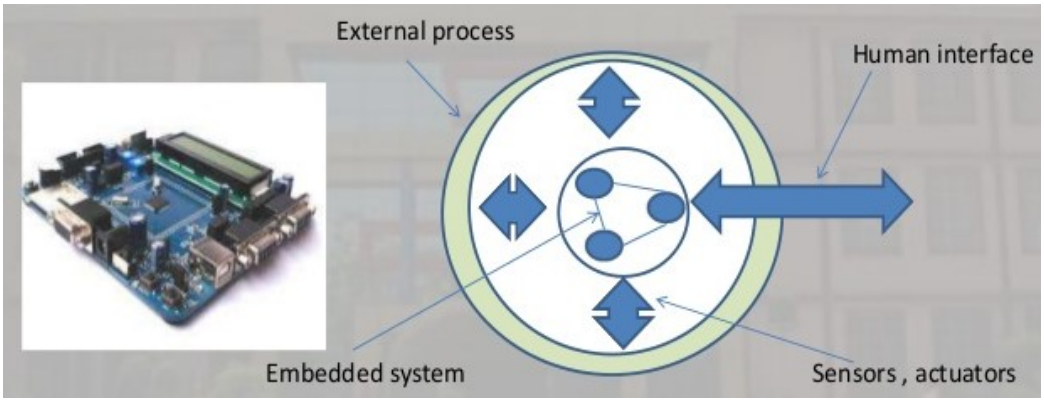


Figure 1.5: Flow diagram for embedded system [41].

It can also perform the functions necessarily for the servo control. For example, in an electric-actuated robot system, the low-voltage control signals are sent out to the motor drive amplifiers to produce power for the motors. Meanwhile, the internal sensors measure the actual position of the motors and sent back to the microcontroller.

Additionally, the software development of an embedded system is closely related to the hardware, which could be tailored to make the system suitable for various robot applications. Typically, four electric-actuated quadruped robots with key specifications are presented in Table 1.2.

## 1.3 Objectives and Contributions

### 1.3.1 Objectives

To develop a dynamic and versatile quadruped robot, powered by electric actuators, the objectives of the project are summarized as follows:

- ***Design of a robot experimental platform***: Firstly, we intend to develop the robot embedded system, including the onboard hardware and software co-design. By integrating the designed embedded system, actuators and sensors, the robot experimental platform is then constructed.

- ***Control of joint motion and leg locomotion***: Based on the first objective, we aim to design and apply the control algorithm to test the joint motion and to further manipulate each leg to complete certain locomotion and gestures.

The goal of present thesis is to make a contribution toward the achievement of the above objectives. This thesis describes the design and development of an embedded system for joint motion control in details. Moreover, it provides a foundation for further improvement and implementation of the robot platform and locomotion control. In addition, it also provides a reference for people conducting research within the project and its collaborators.

### 1.3.2 Contributions

The main contributions of the thesis project are listed below:

- The hardware of the robot embedded system is designed to provide the underlying platform for motor control.

- The software of the robot embedded system is developed in Keil uVision IDE and programmed into a STM32 microcontroller.
- Based on the designed embedded system, actuators and sensors are then tested and selected to set up the robot experimental platform.
- The moving average filter based cascaded PID control strategy is designed and implemented on the closed-loop joint motion system.
- Existing mechanical design problems are analyzed and possible solutions regarding motor torque transmission are proposed to further improve the joint structures.

## 1.4 Thesis Organization

The remainder of this thesis is organized as follows:

- **Chapter 2** introduces the robot system specifications, joint structures, and the principles of leg motions. In addition, the research development process is reported based on the predefined objectives.
- **Chapter 3** presents the hardware design of the embedded system in details, with descriptions of robot component selections. Next, the circuit schematic diagrams and PCBs in two versions are discussed and analyzed with comparisons.
- **Chapter 4** studies the robot joint motion system, based on the testing of sensors and actuators, firmware configuration and software development. By implementing the MAF-based cascaded PID control strategy, experimental results are shown with respect to the motion performance of both knee and hip joints.

- **Chapter 5** summarizes this thesis with the conclusions and future research directions.

Table 1.2: Key specifications of four electric-powered quadruped robots.

| Type / Index | Laikago | Mini Cheetah | Jueying | SpotMini |
|---|---|---|---|---|
| Dimensions (L×W×H;cm) | 55×35×60 | 48×27×30 | 85×50×65 | 84 (H) |
| Weight (kg) | 22 | 9 | 40 | 30 |
| DOF | 12 | 18 | 12 | 17 |
| Speed (km/h) | 2.88 | 8.8 | ≥7 | 5.76 |
| Actuators | customed BLDC motors | electric motors | customed PMSM motors | all-electric |
| Sensors | IMU, joint encoders foot force sensors | IMU hall-effect encoders | IMU, lidar,camera foot force sensors | IMU, camera position/force sensors |
| Power | lithium-ion battery | lithium-ion battery | lithium-ion battery | lithium-ion battery |
| Runtime (h) | 3-4 | 2 | 2-4 | 1.5 |
| Computing | ARM processors, extra PC | STM32F4 MCU, Intel processor | Intel Core i7 | custom control computing system |
| Software | Ubuntu Linux OS | Linux OS | QNX | GRPC-based API Python client library |
| Application | Research, Industrial | Research | Research, Industrial | Research, Industrial |

# Chapter 2

# Robot Specifications and Mechanical Structure

## 2.1 Introduction

This chapter presents the overall specifications and the mechanical structure of the quadruped robot. Firstly, the robot specifications in terms of mechanical and electronic properties are introduced in Section 2.2. Then the robot structure is shown in 2.3, with focus on the kinematic structure, torso and legs. To further explain two common walking patterns, principles of the robot leg motion are analyzed based on the structures of hip and knee joints. Furthermore, a development process of the thesis project is given in Section 2.4.

## 2.2 Robot Specifications

The robot mechanical structure is mainly built in a high-strength aluminum alloy and stainless steel. Each leg features 3 DOFs and has compliance to moderate foot-ground impact. The joints are fully actuated by 12 Maxon DC motors; each rotation

angle is measured by a potentiometer and controlled by a STM32F4 microcontroller. The 3D-CAD model of the robot with components description is shown in Figure 2.1. The key specifications of the quadruped robot are summarized in Table 2.1.

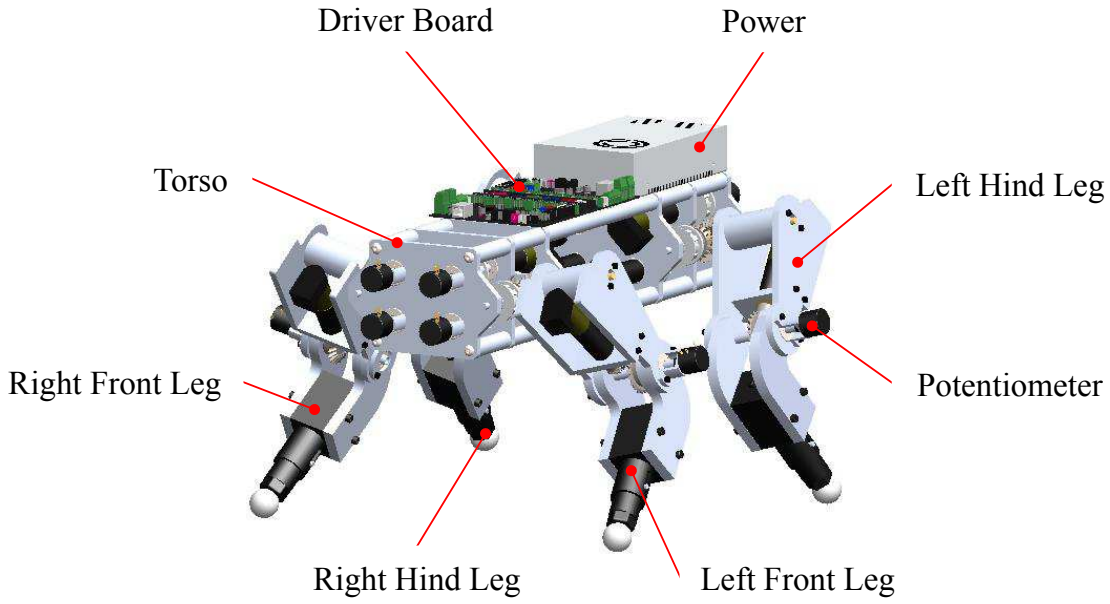


Figure 2.1: Robot 3D-CAD model with components description.

Table 2.1: Key specifications of the designed quadruped robot.

| Specification | Value |
|---|---|
| Dimensions (L×W×H;cm) | 52×15×10 |
| DOF | 12; 3 per leg |
| Weight (kg) | 8.8 |
| Leg spring compliance (N/m) | 5250 |
| Joint range of motion (°) | 200 |
| Motor drive | L298N |
| Actuators | Swiss Maxon DC motor |
| Sensors | potentiometers, IMU |
| Computing | STM32F407VET6 |
| Software | Keil uVision5 with custom C code |

## 2.3 Robot Structure

### 2.3.1 Kinematic Structure

The quadruped robot has four identical compliant legs. They are mounted to the torso in a way that the pitching joints of the front and hind legs face each other, as shown in Figure 2.2. Each leg features three active DOFs, with two lying on the shoulder part (hip joint) and one on the knee joint. In addition, the robot components with their weight are listed in Table 2.2, including the torso, legs, controller board and power supply.

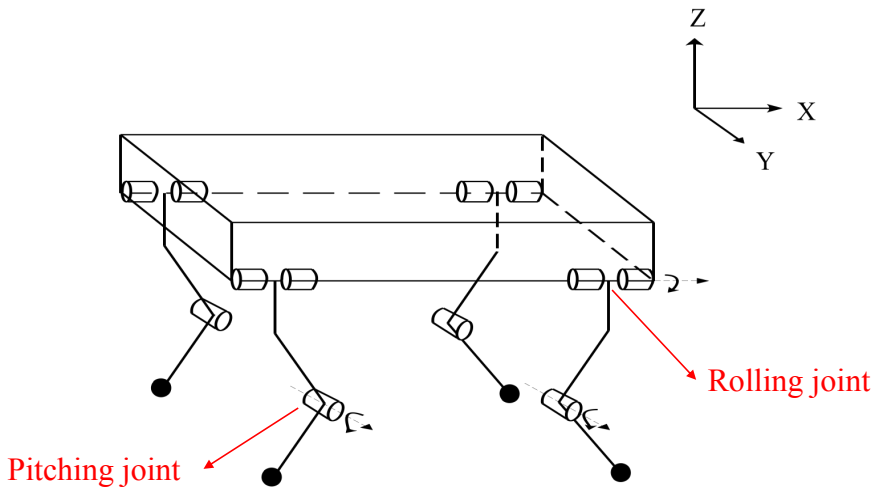


Figure 2.2: Kinematic structure of the robot with hip and knee joints.

Table 2.2: The weight of the robot components.

| Component | Weight (kg) |
|---|---|
| Torso | 4 |
| legs | 4 |
| Controller board | 0.3 |
| Power supply | 0.5 |
| Total weight | 8.8 |

### 2.3.2 Torso

The torso, is designed not only to carry most of the robot components, but also to provide a rigid platform for four legs to be easily mounted. In order to achieve weight reduction and balance of the robot, some lightweight components are utilized and symmetrically assembled on the main body. To ensure the construction materials to be strong and impact-resistance, most parts of the robot including the torso, are constructed by aluminum alloys 6061 that features high strength and toughness. The main torso components are listed in Table 2.3.

Table 2.3: Torso components of the quadruped robot.

| Component | Quantity |
|---|---|
| Swiss Maxon DC motor 41.022.022 | 8 |
| Sakae 22HP-10 Potentiometer | 8 |
| Aluminum plates | 6 |
| Timing belt | 8 |
| Bevel gear | 8 |
| Pulley | 16 |

### 2.3.3 Legs

Among all components of the robot, legs are the most important parts. The properties, such as the weight, dimensions and joint actuation, will directly influence the motion performance of legs and therefore the robot. Each leg consists of a hip joint, thigh, knee joint, shank and a foot for ground contact.

The brass shaft is fixed along the motor shaft by a set of screw, and expected to rotate synchronously with the motor. Pulley 1, sleeved on the brass shaft, is connected to the pulley 2 via a timing belt to transfer the torque from the motor to the pin joint. Different from the common structure in [42, 43] , three identical bevel

gears are assembled vertically to each other on the pin joint. Pulley 2 and bevel gear 1 (defined as pair A) are expected to rotate in the same pace, as well as pulley 3 and bevel gear 2 (defined as pair B). The mechanical structure of the hip joint is shown in Figure 2.3.

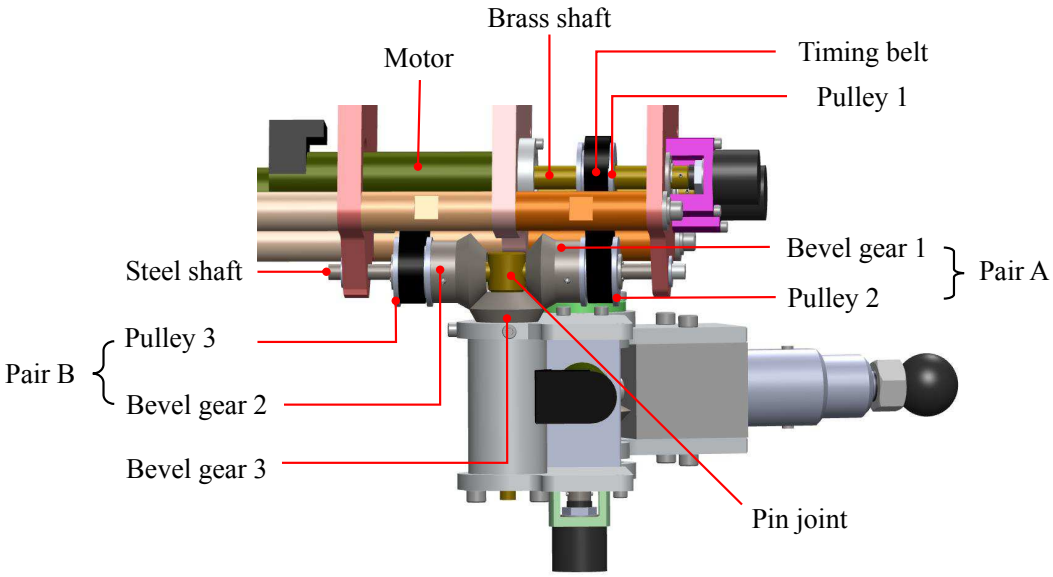


Figure 2.3: CAD model of the hip joint.

The knee joint rotates forward and backward along the vertical plane with only one DOF. The bevel gear 4 is fixed by a screw along the motor shaft. Meanwhile, the bevel gear 5 is mounted vertically on the steel shaft and utilized to connect the thigh rails. The actuation of knee joint is achieved by applying bevel gear 4 and 5 to transmit the driving force from the motor to the foot. Figure 2.4 illustrates the structure of the knee joint.

Based on the structure of hip and knee joints mentioned above, leg motion is then analyzed, which plays an essential role in the experimental testing and further mechanical structure improvement. Intuitively, the hip joint is capable of rotating forward and backward, and can also realize the movement of abduction and adduction. When the bevel gear pairs A and B rotate in the opposite direction, and consequently,

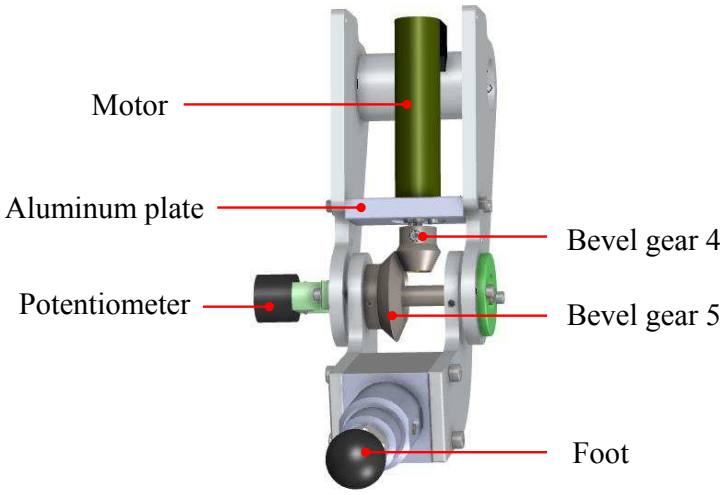


Figure 2.4: CAD model of the knee joint.

the bevel gear 3 will drive the hip joint to rotate back and forth. On the contrary, when the bevel gear pairs A and B rotate in the same direction and speed, the bevel gear 3 will be locked along the pin joint and the thigh part will swing inside and outside. Therefore, different gestures and leg locomotion of the quadruped robot can be realized by cooperation between pair A and pair B. Two common walking patterns of the quadruped robot are presented in Figures 2.5 and 2.6.

- Moving forward and backward

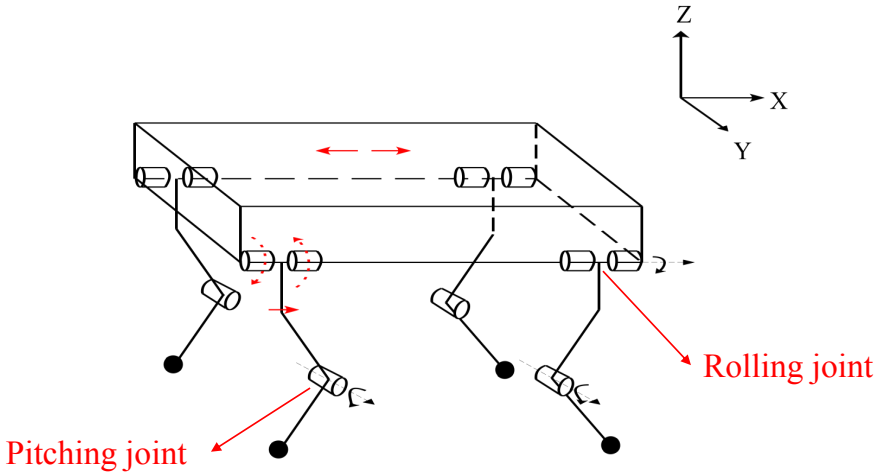


Figure 2.5: Forward and backward movement of the robot.

- Moving left and right

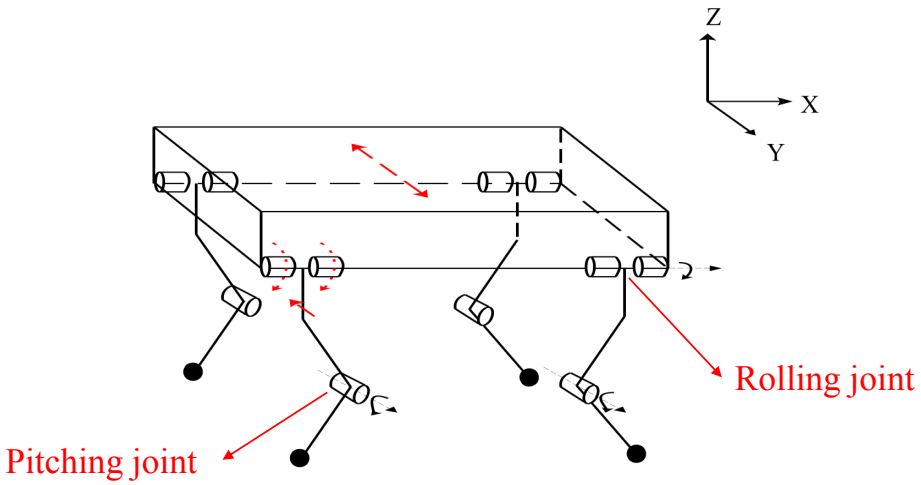


Figure 2.6: Lateral movement of the robot.

## 2.4 Main Stages of the Robot Development

This quadruped robot was originally designed and assembled with only the mechanical structure, aiming at research purposes. However, the robot experimental platform and motion testing were not developed and implemented. Therefore, the structural rationality and locomotion feasibility of the robot were not verified.

To achieve the previous objectives mentioned in Chapter 1, we therefore decided to divide the robot development process into 4 stages in sequence:

- Stage 1: Embedded system hardware design and firmware configuration.
- Stage 2: Software development and hardware testing.
- Stage 3: Component screening and mechanical assembly.
- Stage 4: Control strategy implementation and joint motion experiment.

## 2.5 Conclusions

The quadruped robot has the following torso dimensions of 52cm×15cm×10cm (L×W ×H) and weighs 8.8kg in total. After a brief system overview, the mechanical structure of the robot is discussed systemically including the kinematic structure and descriptions of torso and leg. Next, the geared architecture of hip and knee joints are discussed to specify the leg motion principles. Each joint is actuated by a Swiss Maxon DC motor that provides relatively low speed and high driving torque. In addition, two types of walking patterns are illustrated based on the collaboration of bevel gears. The chapter ends with a development procedure of the project, which will be discussed in the following chapters.

# Chapter 3

# Embedded System Hardware Design

## 3.1 Introduction

As a typical type of embedded system, the quadruped robot is characterized by strong correlation between hardware and software. Therefore, during the development of a robotic embedded system, a methodology of hardware/software co-design is emerged frequently to meet system demands in an optimized manner. However, without the basic and essential support of hardware platform, software and experimental tests are meaningless and cannot be further conducted. Moreover, the onboard hardware is usually customized for specific applications, which in turn integrates with a number of heterogeneous components, and thus increases the complexity of the hardware design.

The hardware used to control the quadruped robot went through two versions, which are both designed in Altium Designer [44]. The first version of the driver board consists of all the required components with H-bridge circuitry symmetrically distributed on both sides of the board. Unfortunately, due to the issues brought by

the irrational MCU pin allocation, excessive welding elements, and improper bypass components, the chip was damaged by the unexpected current or voltage in the experiment.

Chapter 3 introduces the hardware design of the embedded system. Firstly, we introduce the selection of the main components, including MCU and power supply. Secondly, after illustrating the hardware architecture, we discuss the circuit schematic design for each functional module. Finally, we present and compare two versions of the printed circuit board design. Figure 3.1 shows the appearance of two versions of the PCB.

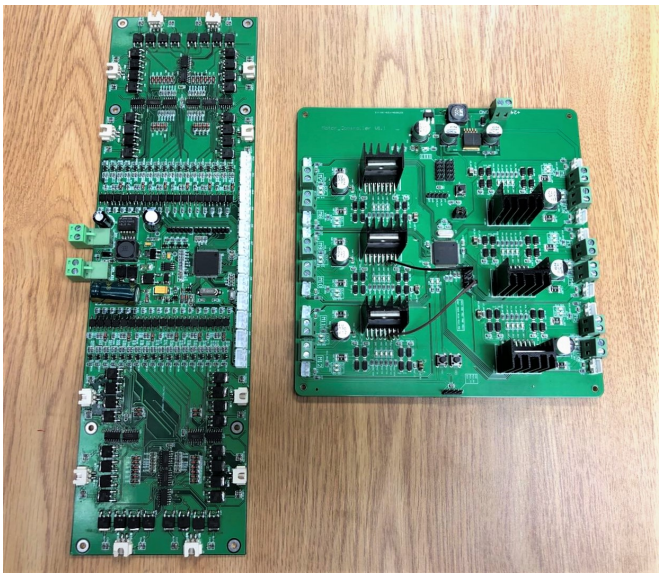

Figure 3.1: First version of the PCB (left) and second version of the PCB (right).

## 3.2 Component Selection

Component selection is an indispensable stage of the embedded system design, which is usually prior or parallel to the software development. In order to build an embedded system fulfilling the requirements, it is important to consider hardware properties, functional requirements and comprehensive marketing research.

### 3.2.1 Microcontroller

A microcontroller is essentially a small computer, running on a single integrated chip. It incorporates the memory, general input/output interfaces, and other peripherals. The related most important factors [45] are shown as follows:

- ***Application***

Our objective is to achieve motor speed and position control. To handle compute-intensive tasks, such as massive A/D conversions and data filtering, which require strong computing capability, we prefer to choose a floating point unit (FPU) for the hardware design to better perform operations involving a lot of decimal numbers.

- ***Clock rate***

Generally, motor control applications use a sampling rate of 100ksps or higher. However, the higher the clock rate is, the more power the system will consume. In addition, the anti-interference performance is inversely proportional to the MCU operating speed. Therefore, an MCU that features high clock rate with low power consumption is definitely ideal. For our case, 12 DC motors are controlled in parallel, which requires the sampling rate to be greater than 1Msps.

- ***Number of pinout and I/Os***

Generally, a hardware block diagram is utilized to enumerate all the external interfaces supported by the MCU. There are two types of interfaces which are commonly listed. The first type is the communication interface, which affects the program space of the MCU, i.e., USB, SWD, UART, etc. The second type is the digital inputs/outputs, A/D inputs, PWM, etc. The two types of interfaces straightly dictate the number of I/O pins required by the microcontroller. Figure 3.2 illustrates the hardware block diagram of the MCU with required I/Os.

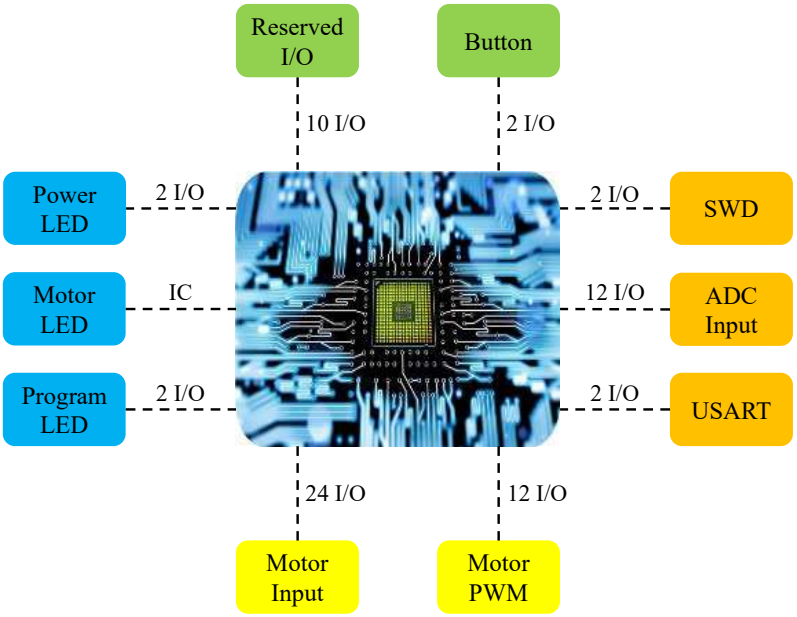


Figure 3.2: Block diagram of MCU with required I/Os.

- ***Memory requirements***

There are three different types of memory associated with an MCU: Flash, SRAM and EEPROM. The required memory depends on the size of the software. However, it might not be easy to evaluate and instead, the workload of the MCU can be estimated and predicted. For our case, it is critical to ensure that the program space is enough, as the amount of code containing real-time applications and data optimization is relatively large. The MCU with medium or large size memory is relatively suitable in our hardware design.

- ***Bit size***

Selecting an MCU with proper bit size is another basic requirement. For instance, using an unsigned integer requires 16-bit of memory due to the data type. However, the most significant byte may be lost if the data is executed on an 8-bit MCU. For our case, the bit size of the MCU should be at least 16-bit, thus 32-bit MCU is the

most proper choice. Figure 3.2 illustrates the embedded market share of processors in terms of bit size, researched by global electronics industry magazine "EE Times".

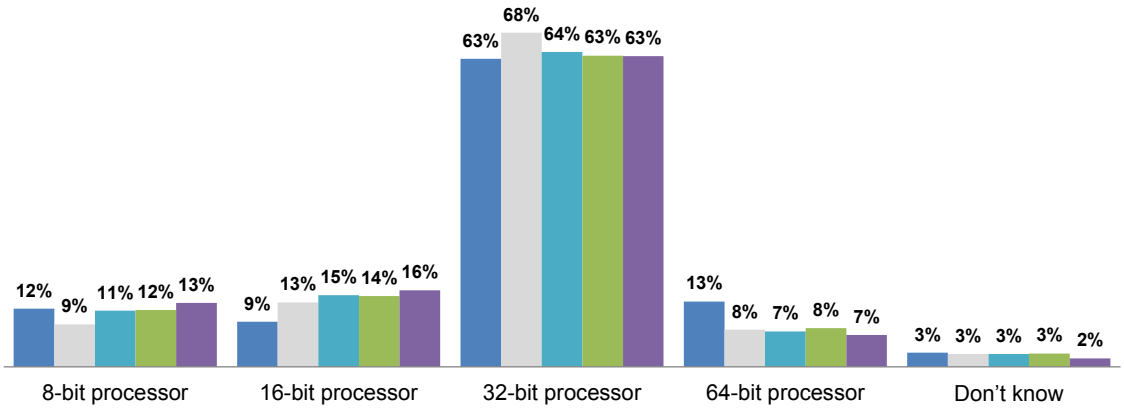


Figure 3.3: Main processor bit size in 2017 embedded markets study [46].

- ***Development tools, cost and compatibility***

It is prior to use an MCU with resourceful toolkit, i.e., data sheet, code samples, and preferably a large online community, which can reduce the development time. Meanwhile, it is necessary to reduce the cost of components and the entire project as much as possible on the premise of guaranteed performance. In our design, the compatibility of MCU is also considered. To realize the hierarchical communication between high-level and underlying controller, the chip is required to work harmoniously on at least two development platforms with assistance of compatible firmware.

Furthermore, some general principles of chip selection are listed as follows. Firstly, to reduce energy consumption and extend the equipment life cycle, we prefer to use low power MCU. Moreover, the chip with 'QFP' package is often adopted for products with limited size, thereby reducing costs while simultaneously contributing to electromagnetic compatibility (EMC) design.

Based on the above evaluation criteria, the minimum requirements of the ideal MCU in terms of the performance specifications are summarized in Table 3.1.

Table 3.1: Specification requirements of the microcontroller.

| Index | Value |
|---|---|
| Pin count | ≥80 |
| I/O count | ≥68 |
| ADC pin count | ≥12 |
| Clock rate (MHz) | ≥48 |
| Bit size (bit) | ≥16 |
| Sampling rate (Msps) | ≥1 |
| Flash size (KB) | ≥512 |
| SRAM size (KB) | ≥64 |
| ADC resolution (bit) | 12 |
| Supply voltage (V) | 1.8-5.5 |
| Cost (USD) | ≤10 |

The MCU is essentially chosen from the various semiconductor manufacturers. After conducting the MCU marketing research in the field of motor control and real-time data processing, 5 MCUs were finally taken into consideration, as illustrated in Table 3.2.

The selection of MCU is conducted according to the following two steps:

- We first pick out the candidates that satisfy the minimum requirements by comparing each indicator between the product and ideal MCU.
- Among the rest candidates, we estimate and screen out the most suitable MCU, based on the key specifications, compatibility and the cost.

Table 3.2: Comparison of specifications of 5 MCUs.

| Index \ MCU | Infineon XMC1302 | Microchip SAMC21N18 | Microchip SAMD51N20 | STMicroelectronics STM32F407VET6 | Texas Instruments TMS320F28335 |
|---|---|---|---|---|---|
| Core | ARM Cortex-M0 | ARM Cortex-M0+ | ARM Cortex-M4F | ARM Cortex-M4F | DSP C28x |
| Pin count | 40 | 100 | 100 | 100 | 176 |
| I/O count | 34 | 84 | 81 | 82 | 88 |
| Clock rate (MHz) | 32 | 48 | 120 | 168 | 150 |
| Sampling rate (Msps) | 0.75 | 1 | 1 | 2.4 | 12.5 |
| Bit size (bit) | 32 | 32 | 32 | 32 | 32 |
| Flash size (KB) | 200 | 128/256 | 1024 | 1024 | 512 |
| SRAM size (KB) | 16 | 16/32 | 256 | 192 | 68 |
| ADC resolution (bit) | 12×1 16 CHx | 12×2 20 CHx | 12×2 20 CHx | 12×3 16 CHx | 12×2 16 CHx |
| Supply voltage (V) | 1.8-5.5 | 1.6-5.5 | 1.7-3.6 | 1.8-3.6 | 1.8-3.3 |
| Package | VQFN-40 | TQFP-100 | TQFP-100 | LQFP-100 | LQFP-176 |
| Interface type | SPI, UART $I^2C$, $I^2S$ | SPI, UART $I^2C$, CAN | SPI, UART $I^2C$, CAN | SPI, UART/USART $I^2C$, $I^2S$, SDIO, USB | SPI, UART $I^2C$, CAN |
| FPU | N/A | N/A | ✓ | ✓ | ✓ |
| Development tools | ✓ | ✓ | ✓ | ✓ | ✓ |
| Compatibility | ✓ | ✓ | ✓ | ✓ | ✓ |
| Cost (USD) | 3.91 | 3.84 | 6.17 | 4.77 | 14.25 |

In the first stage of selection, the XMC1302 and SAMC21N18 chips are excluded. It is obvious that the number of I/Os, sampling rate and the memory size of XMC1302 cannot meet the minimum requirements. Moreover, most specifications of SAMC21N18 meet the basic requirements. However, the memory size is relatively small. The program cannot be downloaded into the MCU completely and the follow-up tasks are not able to be executed if the memory size is smaller than the program size.

In the second stage of selection, the rest three candidates all meet the requirements and therefore we further compare the key specification among each other. These specifications should be clarified and served as decision factors to screen out the MCU more effectively. The clock and sampling rate are important for real-time data processing and motor control. ST chip has the highest clock rate at 168MHz, while TI chip has the fastest sampling rate at 12.5Msps, much faster than the other two. In terms of memory size, TI chip has only 512KB flash, while Microchip and ST chip has 1MB flash. Furthermore, abundant peripheral interfaces and compatibility with ROS [47] framework are also required. In addition, the cost cannot be neglected. Although TI chip is the best at handling complex computation among these three chips, however, its price is 3 times than that of ST chip. As a result, it is also excluded.

Ultimately, the STM32F407VET6 is chosen as the main processor for hardware design, with its large memory size, sufficient interfaces, and the lowest cost.

### 3.2.2 Power Supply

The operating voltage of each circuit component is not the same. Therefore, voltage converter should be used in our hardware circuit design. The power electronics converter can be classified into AC/DC converter [48], DC/AC converter, AC/AC

converter, DC/DC converter [49]. These converters can be also divided into buck or boost converters [50]. There are two approaches to regulate the low DC voltage to the final rail voltage: Utilizing either an LDO [51] or a DC/DC switching converter. The LDO can be only used in buck applications, while the switching regulator can either be designed to boost or buck the output, or even do both seamlessly.

When the voltage difference between input and output is very large, the switching regulator is always the first choice, primarily due to its high efficiency. However, If the input and output voltages are close, the LDO is often adopted, because its inefficiency relative to the switcher is often negligible and switching noise is not generated. The differences between these two types of regulators are shown in Table 3.3.

Table 3.3: Comparison of the characteristics of LDO and switching regulators.

| Type / Index | LDO converter | Switching regulator |
|---|---|---|
| Conversion efficiency | Low | High |
| Ripple wave | Small | Big |
| Noise | Low | High |
| Function | Buck | Boost/Buck, Buck-Boost |
| Application scenario | Buck circuit<br>Power isolation<br>Filtering | Boost/Buck circuit<br>Charge pump<br>Inductive energy storage |
| Size | Small | Large |
| Complexity | Low | High |
| Heat generation | High | Low |
| Cost | Low | Relatively high |

To design the power supply module, we purpose three possible solutions as follows:

- Solution 1: 24V to 5V, 5V to 3.3V LDO regulator.
- Solution 2: 24V to 12V, 12V to 5V, 5V to 3.3V LDO regulator.
- Solution 3: 24V to 5V switching regulator, 5V to 3.3V LDO regulator.

In Solution 1, the 24V/5V LDO is relatively not common. More importantly, there is a 19V voltage drop during the conversion. When the power supply current reaches 100mA, the dissipation power is 1.9W, which will heat up the MCU severely. In Solution 2, the cost is much higher and the overall power loss is also large. In Solution 3, the switching regulator has a large voltage regulation range with a small energy loss. Meanwhile, the LDO is used to drop the voltage from 5V to 3.3V, which can guarantee the performance with reasonable cost. In conclusion, solution 3 is finally adopted. Figure 3.4 illustrates the power distribution of the quadruped robot.

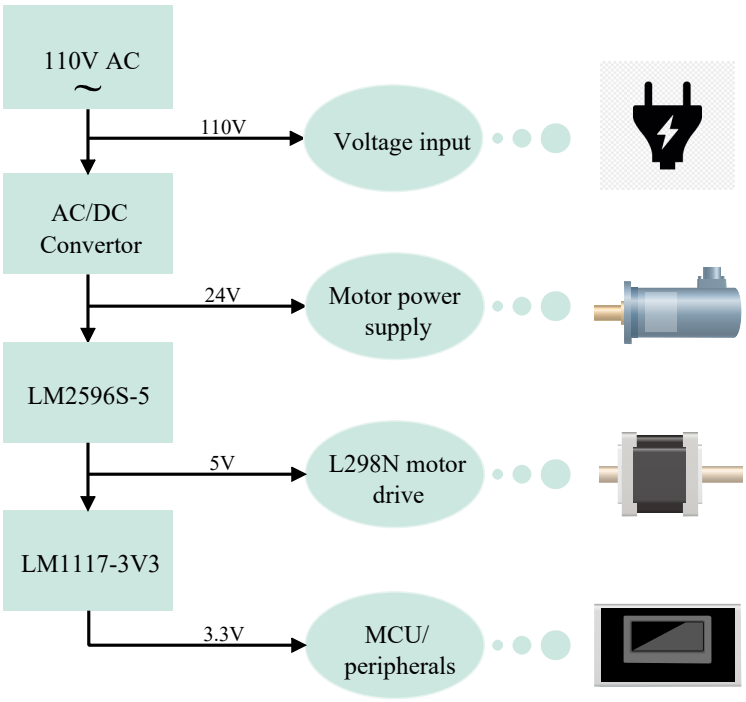


Figure 3.4: Power distribution of the quadruped robot.

The power supply of the quadruped robot can be divided into three parts: 24V for actuating 12 brushless DC motor, 5V for driving L298N motor drive and 3.3V for controlling the MCU and peripheral components, respectively. In consideration of convenience and durability of the experiment, an 110/220V-24V AC/DC regulated power supply is adopted, instead of a rechargeable battery.

## 3.3 Circuit Schematic Design

This section presents the circuit schematic design of the embedded system. After determining the overall hardware architecture, the circuit diagram for each functional module is ready to be designed. In order to better illustrate the different design methods and improvements of the two versions, circuitry regarding each component will be shown and compared.

### 3.3.1 Hardware Architecture

The modular hardware architecture consists of:

- STM32F407VET6 microcontroller.
- IMU: Measures the real-time attitude angle of the robot.
- Memory: Stores the basic firmware and programs of the control tasks.
- Motor control interface: Connects with the L298N motor drive circuitry.
- Potentiometer: Sends back the analog value of the joint position to the MCU.
- Communication interface: Connects with the PC and downloads the programs.
- Power supply: Provides the power to actuate the DC motors and the circuitry.

Combining these modules, the prototype of onboard hardware is completed. The hardware block diagram of the embedded system is shown in Figure 3.5.

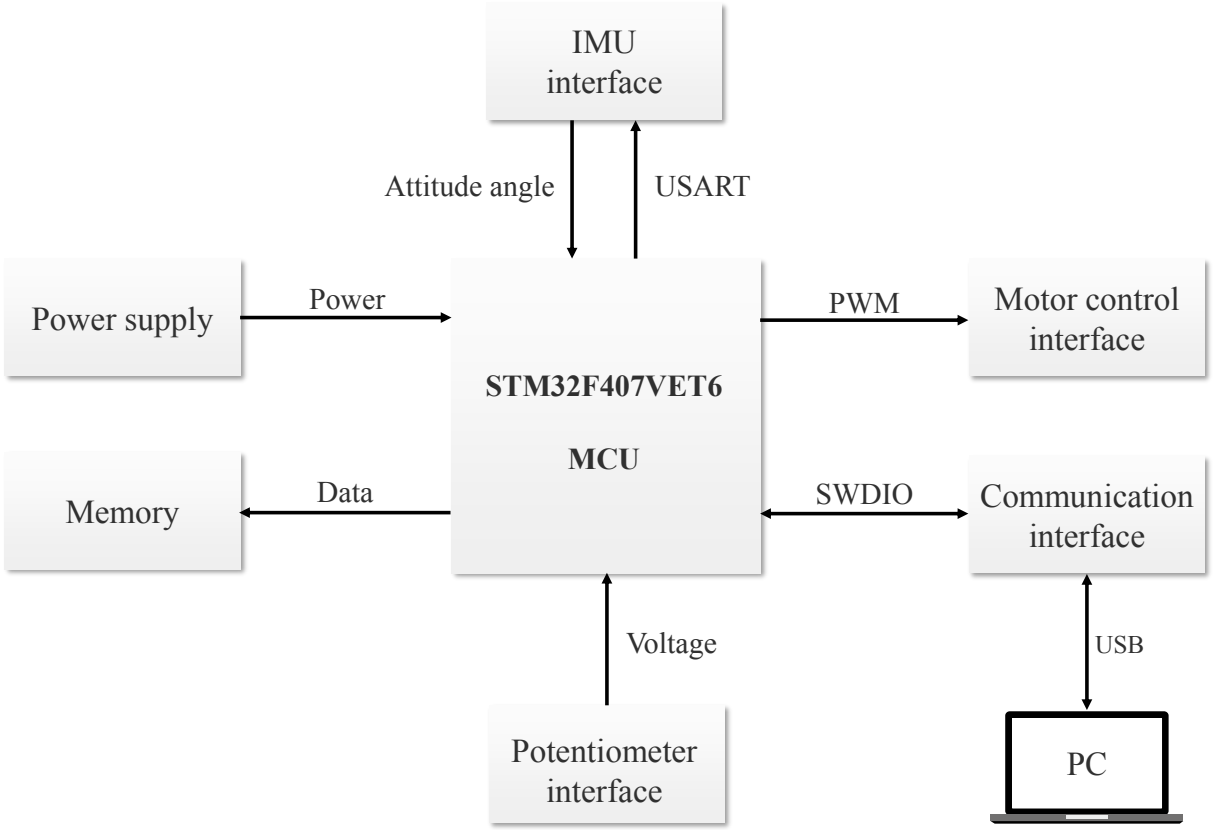


Figure 3.5: The hardware block diagram of the embedded system.

### 3.3.2 Pin Allocation

After selecting the MCU, we further allocate each pin function properly according to objectives, based on the data sheets. Otherwise, it may waste the memory space or even fail to complete circuit schematic design. In addition, pins can be further divided into several types to realize different functions, which are shown as follows.

- ***PWM pin***

The PWM duty cycle is used to vary motor speed by controlling the terminal voltage. As the duty cycle increases, the higher average voltage is applied to the motor, the

faster the motor will rotate. In STM32F4 data sheet [52], timer output pins in compare mode are preferred to generate PWM waveform instead of others.

- ***Analog/Digital pin***

The analog-to-digital pins of MCU are directly connected to the terminal pin of the potentiometer. Hence, the pins with ADC function can be allocated only. To improve conversion accuracy, the ADC has an independent power supply that can be filtered separately, and shielded from noise on the PCB.

- ***SWD pin***

Serial Wire Debug (SWD) provides a debug port for small package MCUs. In order to communicate with a device via SWD, 2 pins are required to connect with the processor: SWDIO pin transmits and receives bi-directional data, while SWCLK pin is used to synchronize the clock signal.

- ***USART pin***

The USART is a microchip that facilitates communication through a computer serial port using RS-232C protocol. The USART pins send the information of robot attitude angle gathered from IMU to the microcontroller.

- ***Power supply/GND pin***

The circuit is powered by a stabilized power supply $V_{DD}$. Meanwhile, the ground pins, such as $V_{SS}$ and $V_{SSA}$ must always be connected to the external power supply. In addition, decoupling capacitors should be also considered to filter out high-frequency noise from the power source.

After assigning each pin functions reasonably, the resource of MCU can be better utilized, which further increases the efficiency of hardware design. Figure 3.6 shows the overall circuit schematic diagram of the microcontroller.

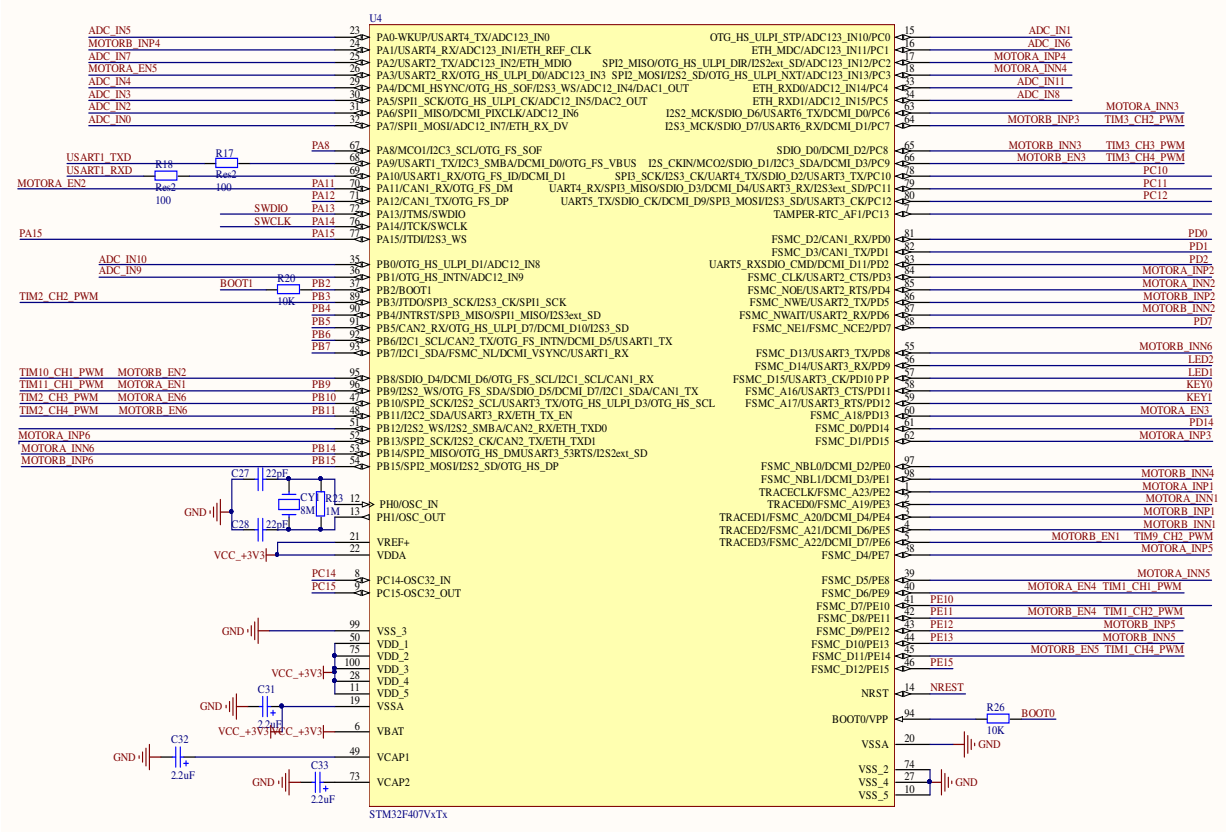


Figure 3.6: Circuit schematic diagram of the MCU.

### 3.3.3 Motor Drive

There are two types of motor drive that are designed to actuate the motors:

- ***MOSFET/Gate driver IC***

In the first version of motor drive, gate driver ICs produce the high-current to rapidly switch on/off power MOSFETs in the bridge circuits. Moreover, the EL357N opto-coupler is placed between the isolated PWM signal and input of NAND gate. Unfortunately, the gate drivers are burnt as voltage exceeded their max value. Figure 3.7 illustrates the motor drive using MOSFETs and gate driver ICs.

However, it is often troublesome to build H-bridges with discrete components. As a result, the size of circuit board and the number of components will largely increase.

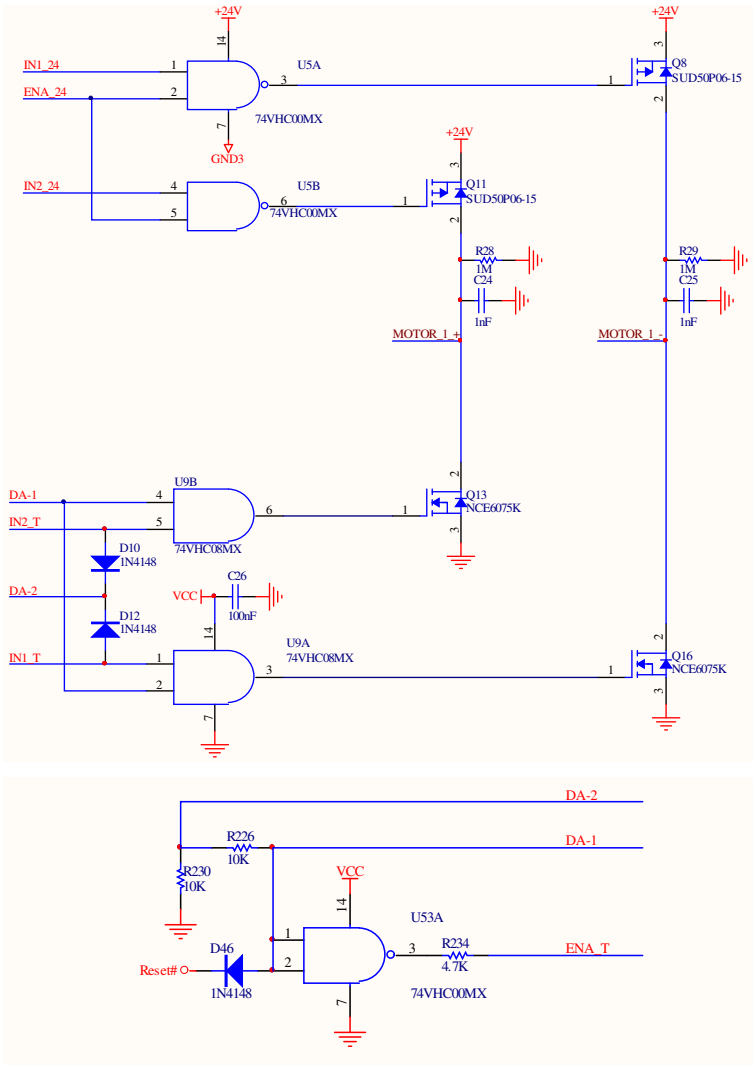


Figure 3.7: First version of the motor drive design.

Considering the fact that the compact motor driver is much more convenient to be applied with lower cost, we finally select the integrated motor drive chip to improve the previous design.

- ***Integrated motor drive chip***

The improved motor drive using L298N is illustrated in Figure 3.8. When the power is off, eight freewheeling protection diodes are set as release paths of self-inductive energy, to prevent the self-inductive voltage from striking through the switching ele-

ment. If the output voltage is greater than 24V, redundant current will flow through diodes to $V_{CC}$, and thus will protect the subsequent circuits. These diodes are selected as fast recovery Schottky diodes that feature fast response [53]. When the DC motor is running, high instantaneous voltage will be generated and the diodes are expected to protect the chip from damage. Additionally, two 1812 fuses are welded at the circuitry of motor output and served as overcurrent protection.

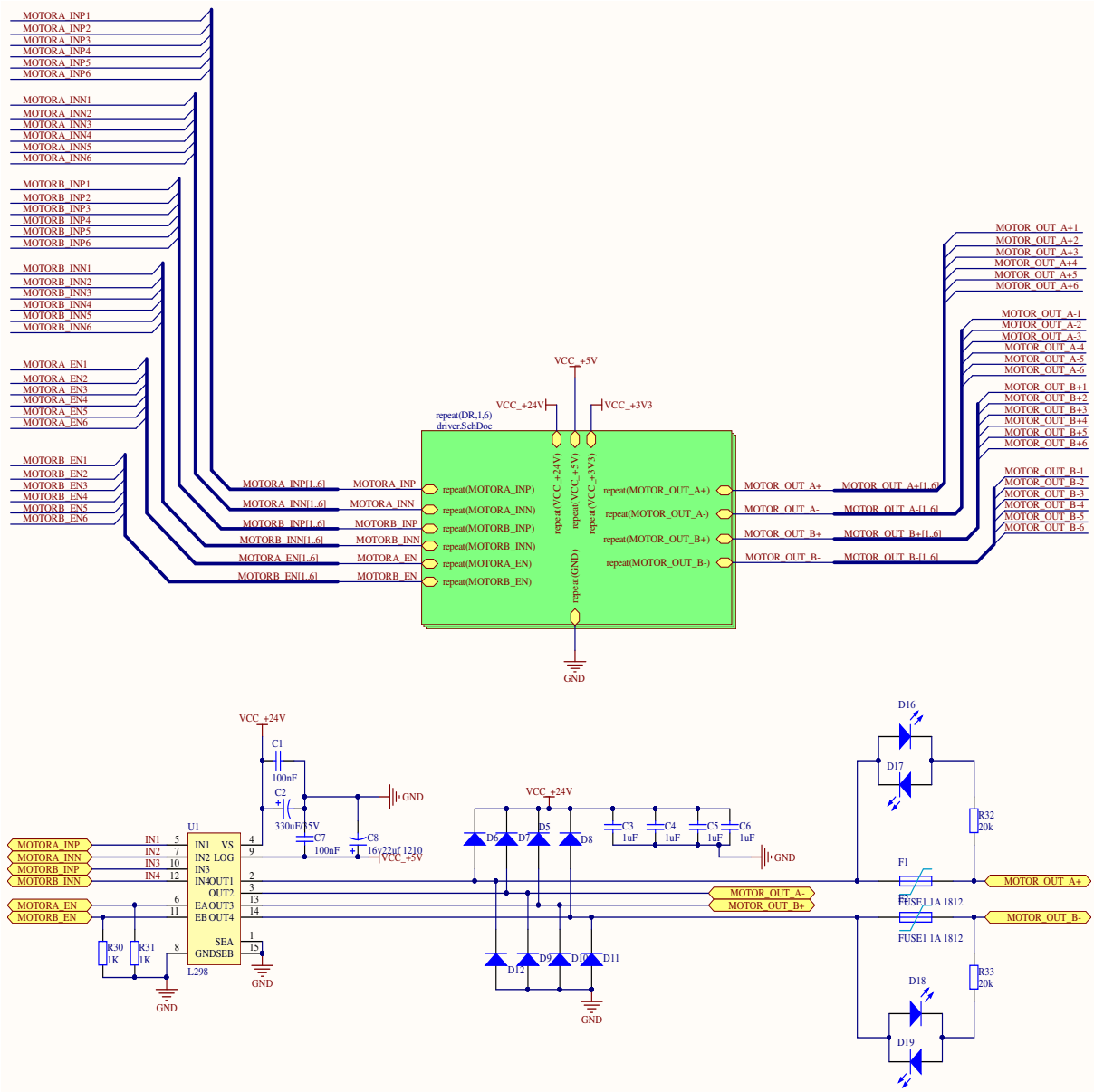


Figure 3.8: Second version of the motor drive design.

### 3.3.4 Voltage Regulation

Originally, the LM2575D2T switching regulator and AMS1117 LDO are utilized. In the experiment testing, however, the regulated output voltages, supposed to be around 5V and 3.3V, are measured about 4.2V and 2.9V with obvious oscillation, which came from the high frequency switching noise. The first version of voltage regulation design is shown in Figure 3.9.

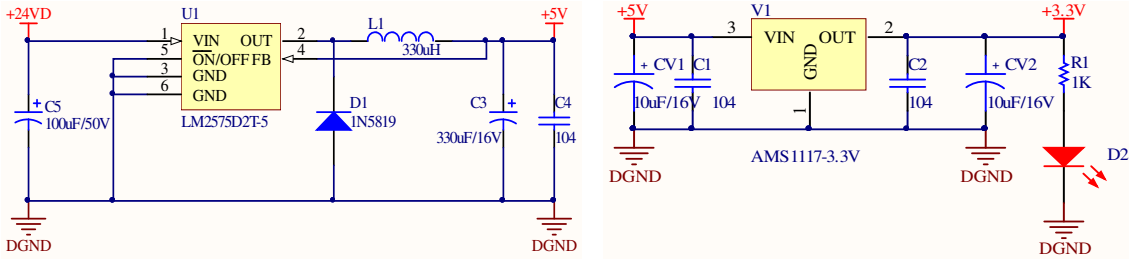


(a) 24-5V regulator LM2575D2T-5. (b) 5-3.3V regulator AMS1117-3V3.

Figure 3.9: First version of the voltage regulation design.

To improve the performance of regulation, the buck switching regulator LM2596S (24V-5V) and LDO LM1117 (5V-3.3V) are finally adopted. They have higher frequency internal oscillator and conversion efficiency, and provide larger current. More importantly, bypass and polar capacitors are added to filter the signal interference and protect the power supply module. Figure 3.10 details the second version of voltage regulation design.

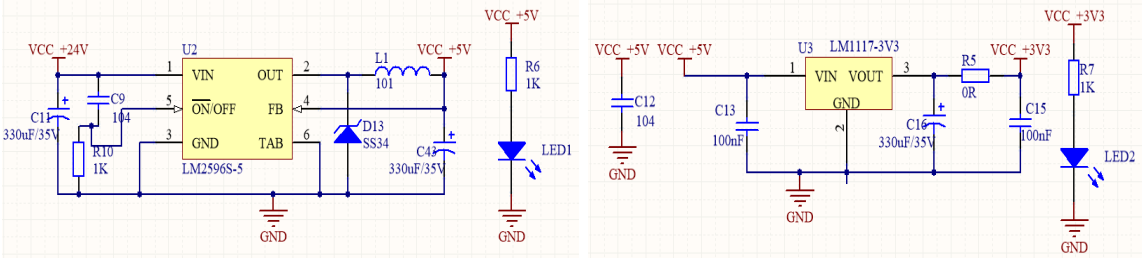


(a) 24V-5V regulator LM2596S-5. (b) 5V-3.3V regulator LM1117-3V3.

Figure 3.10: Second version of the voltage regulation design.

### 3.3.5 Sensor Interfaces

The sensor system of the quadruped robot contains two parts: Potentiometers and IMU. The potentiometer, acting as a type of linear feedback sensor, is used to measure the rotation angle of the motors and send the corresponding analog value to the MCU via specific interface. The design of potentiometer interfaces is shown in Figure 3.11.

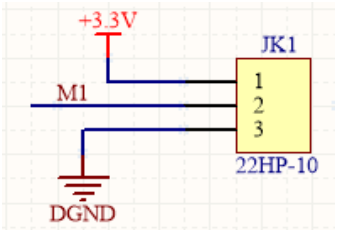


(a) First version of the potentiometer interface design.

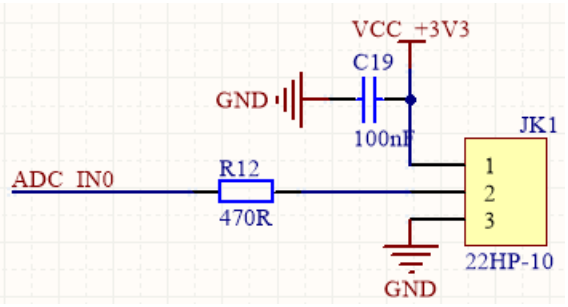


(b) Second version of the potentiometer interface design.

Figure 3.11: Two versions of the potentiometer interface design.

The IMU is installed on the center of torso. It is used to measure and report the acceleration and angular velocity in separate three-axis via accelerometer and gyroscope, and further distinguish the position and orientation of the robot. Furthermore, the information of altitude angles is sent to MCU through USART interface. The design of IMU interfaces is illustrated in Figure 3.12.

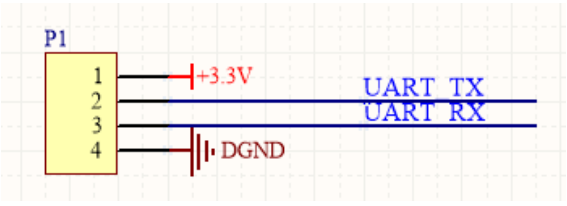


(a) First version of the IMU interface design.

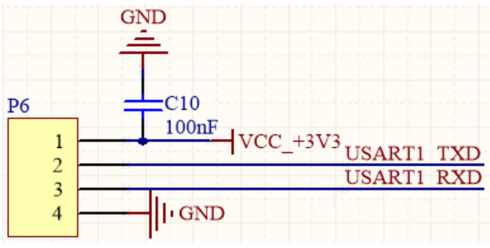


(b) Second version of the IMU interface design.

Figure 3.12: Two versions of the IMU interface design.

## 3.4 PCB Design

### 3.4.1 Overview

The printed circuit board [54] helps to connect the electronics components with pads, tracks and lines incorporated on a laminated copper sheet. The PCB process converts the electronic circuit schematic diagram into a physical circuit board layout, which is widely used in the advanced electronics and automatic control systems. There are mainly three types of PCBs: Single-sided, double-sided and multi-layer PCB, depending on the number of layers used in the boards as well as the practical requirements. PCB is composed of different layers that are joined together with the help of heat and adhesive. The layer structure with thickness descriptions of the designed double-sided PCB is illustrated in Figure 3.13.

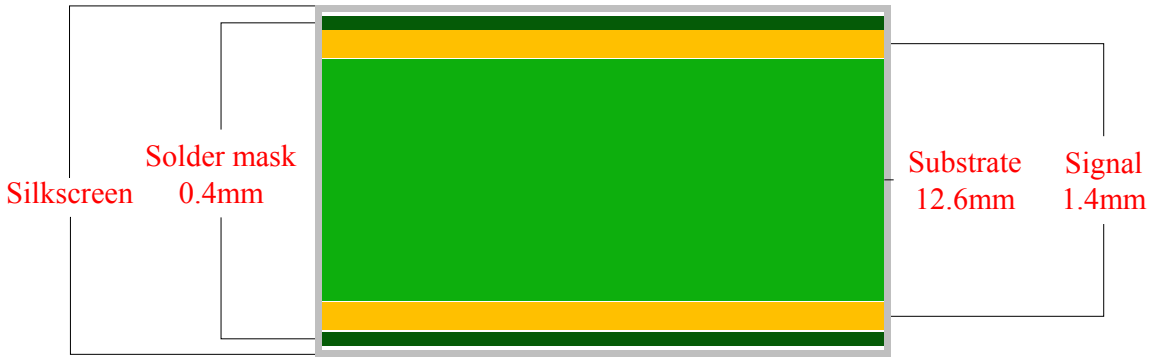


Figure 3.13: Layer structure of the designed double-sided PCB.

- ***Substrate layer***

The substrate layer is composed of fiber glass. In our design, a composite material "FR4" [55], instead of the phenolic resin, is adopted to build a solid substrate, which provides good insulation and rigidity to the PCB.

- ***Signal (Copper) layer***

The signal layer includes top and bottom layers, which is primarily used for placement of components (top and bottom) and routing. The wires or other objects placed on the surface are in the areas covered with copper foil. For double-sided PCB, there are two copper layers, which is applied to both sides of the substrate.

- ***Solder mask layer***

Solder mask contains top and bottom solders, which is most commonly in green. It is overlaid onto the copper layer to insulate the traces from accidental contact with other conductive components. Apart from this, solder mask is also able to prevent copper traces from corrosion, oxidation and dirt.

- ***Silkscreen layer***

Silkscreen is a layer of ink traces that is often applied on top of the solder mask layer. Its main responsibility is to draw letters and identify components, or other text information for easier assembly as well as indicators for better understanding the board.

- ***Mechanical layer***

The mechanical layer defines the appearance of the entire PCB board. It is generally used to set the board's physical dimensions, data markings, assembly instructions, and other mechanical information.

The circuit schematic diagram and PCB layer structures are all designed in Altium Designer. The process flow of PCB design is shown in Figure 3.14.

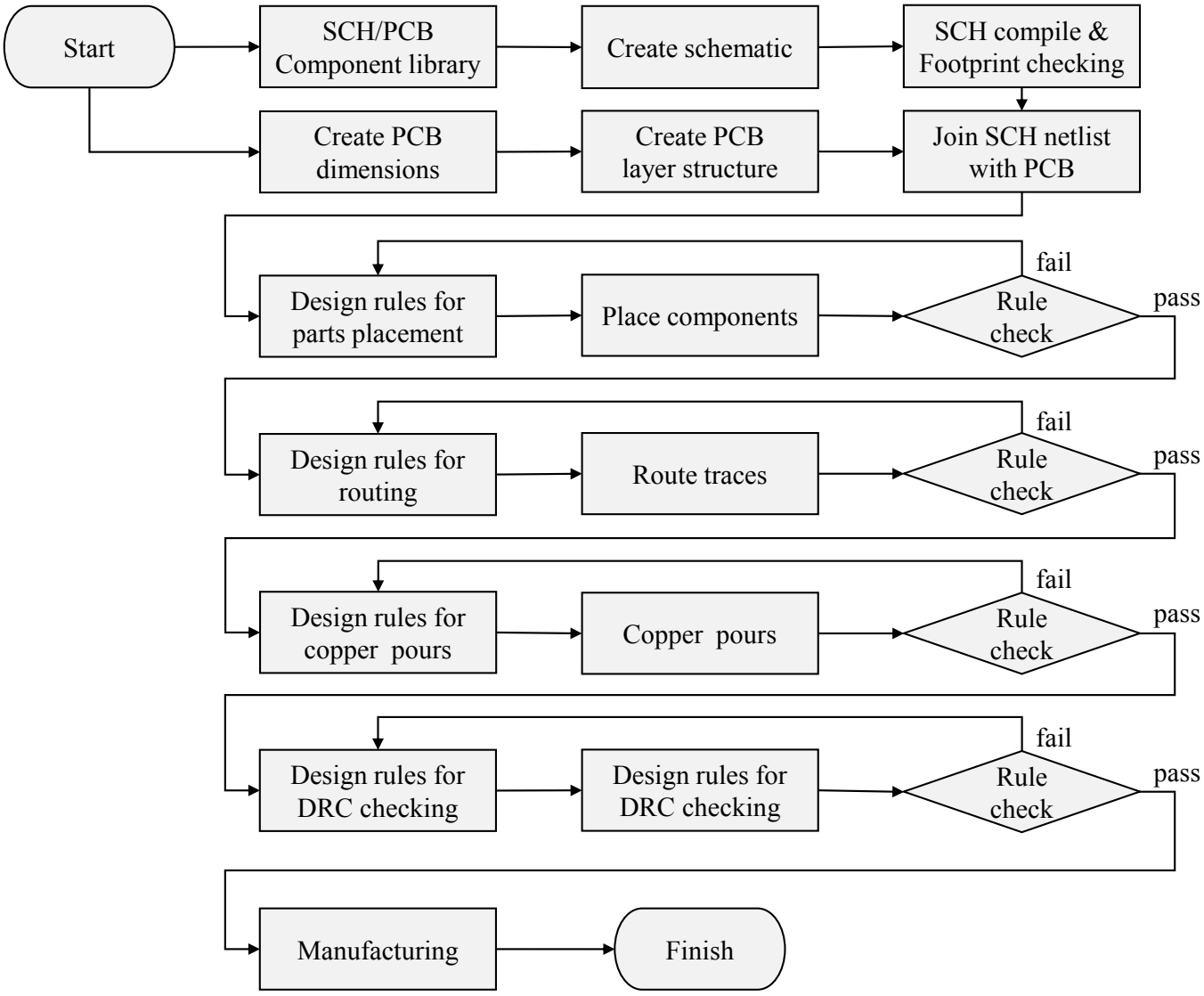


Figure 3.14: Process flow of the PCB design.

### 3.4.2 Power Distribution

In the first version, the MCU is powered by 3.3V and is placed in the center of PCB. To actuate the motor drive, gate driver ICs are driven by the 5V regulated power. The 24V power tracks are routed on the edge of the printed circuit board for actuating 12 DC motors. The original design of the power distribution is shown in Figure 3.15.

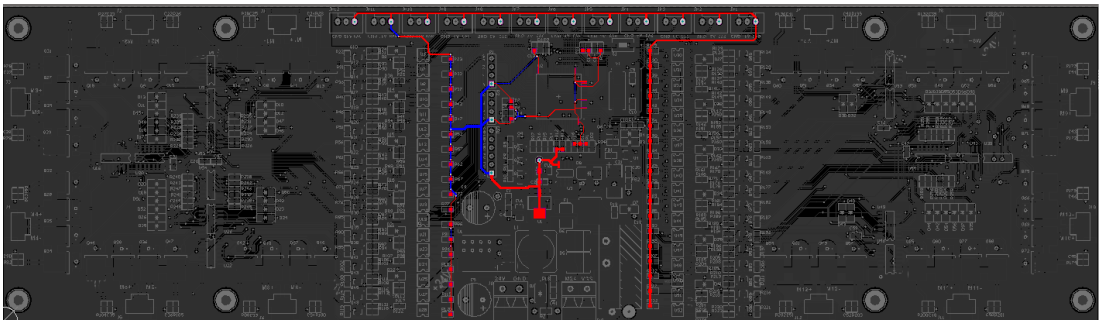

(a) 3.3V for MCU v1.

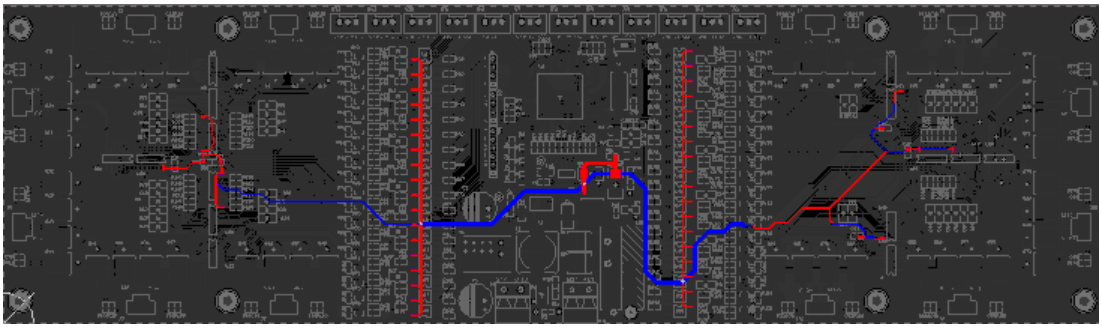

(b) 5V for motor drive v1.

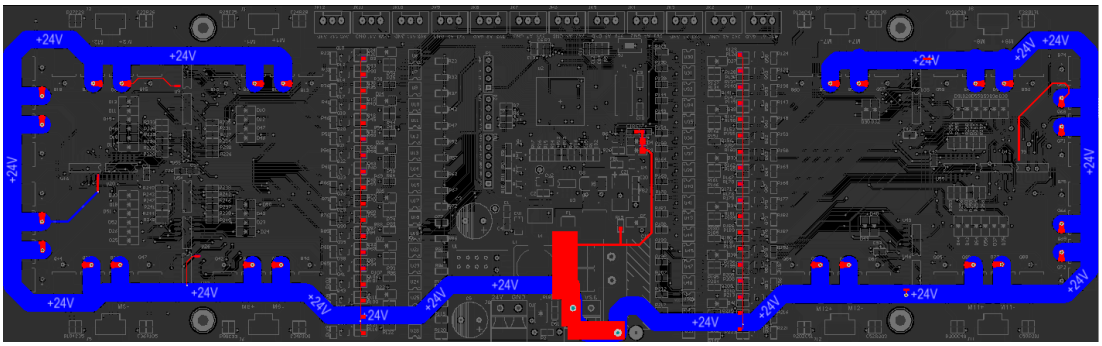


(c) 24V for motor v1.

Figure 3.15: First version of the power distribution design.

In the second version, to mitigate heat dissipation, the physical heat sinks are assembled for each L298N motor drive. Meanwhile, bypass capacitors are utilized to stabilize the output of voltage regulators. Eventually, the redesigned board works perfectly by testing based on more rational components placement and traces routing, as shown in Figure 3.16.

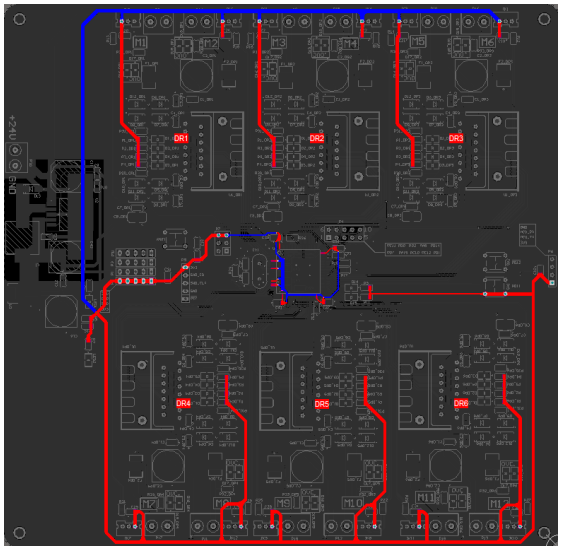

(a) 3.3V for MCU v2.

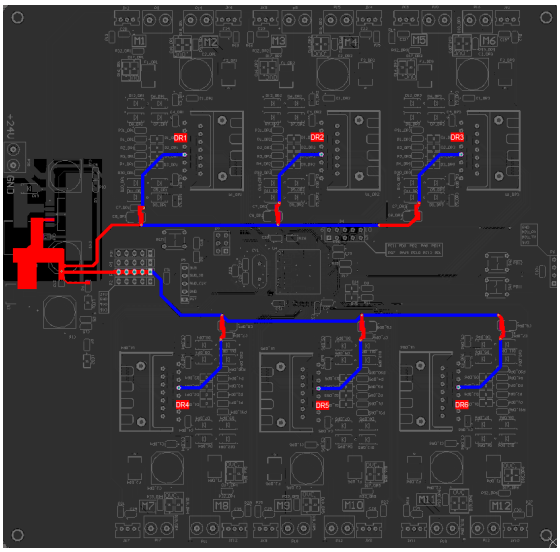

(b) 5V for motor drive v2.

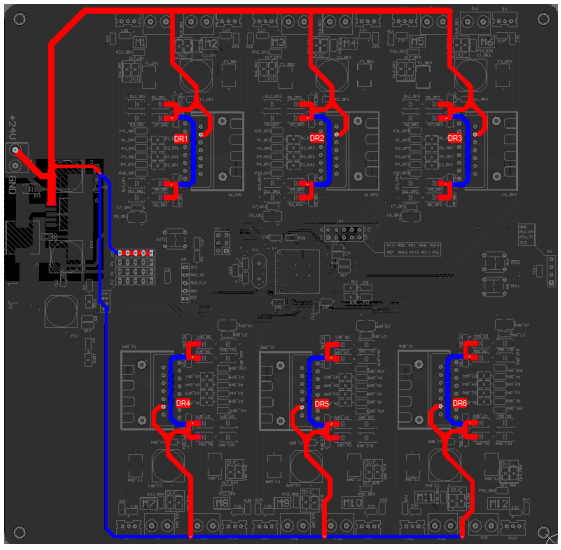

(c) 24V for motor v2.

Figure 3.16: Second version of the power distribution design.

To decrease the parasitic capacitance [56], arising from an electrical coupling between two signal lines or a signal line and the substrate, all the power tracks are distributed symmetrically, and the spacing of each net track is increased properly. The PCB information of two versions design is listed in Table 3.4.

Table 3.4: Comparison of two version of printed circuit board.

| Version / Index | 1st | 2nd |
|---|---|---|
| Dimensions (L×W;cm) | 33.0×9.5 | 17.7×17.3 |
| Component count | 551 | 314 |
| Pad count | 1611 | 869 |
| Track count | 8305 | 4504 |
| Via count | 570 | 220 |
| Net count | 396 | 182 |
| Feasibility | N/A | ✓ |

## 3.5 Conclusions

This chapter details the embedded system hardware design of the quadruped robot, with highlights on the discussion of components selection, circuit schematic design and two versions of PCB. The onboard components are firstly selected based on practical requirements and marketing research. By specifying the overall embedded hardware architecture, the circuit diagrams of each functional module are introduced. Next, the layer structures and process flow of the designed board are illustrated. Finally, the comparison of two versions of PCB in terms of power distribution and onboard specifications is presented.

# Chapter 4

# Joint Motion System Design and Tests

## 4.1 Introduction

This chapter presents the experimental studies that have been conducted during the development process of the robot joint motion system. These studies are centered on the hardware testing, software design and joint motion experiments in Section 4.2, 4.3 and 4.4, respectively. Since the hip joints are not yet fully operational, mechanical structural problems and solutions are given in Section 4.5.

In the first study, the potentiometers and motors are tested and used to setup the system experimental platform. In the second study, the moving average filter based cascaded PID control strategy is designed, aiming to control the motor position and speed, meanwhile, smooth out the random noise in the process of sensor data acquisition. Finally, the designed control algorithm is implemented on two types of joints and the corresponding control performance is tested. The experimental platform of the quadruped robot is shown in Figure 4.1.

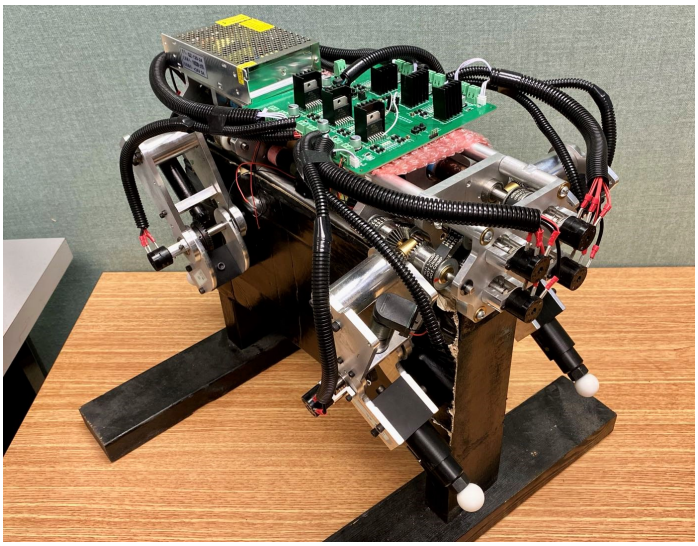

Figure 4.1: Experimental platform of the quadruped robot.

## 4.2 Hardware Tests

In addition to the designed embedded system, as mentioned in Chapter 3, the potentiometers and motors are essential devices that are further tested and selected to constitute the robot experimental platform.

### 4.2.1 Potentiometer Selection

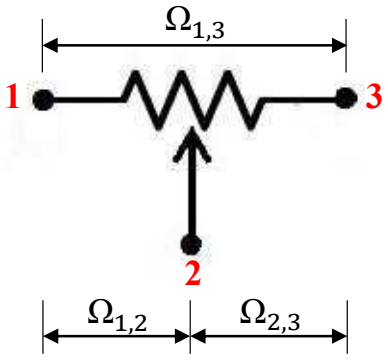


(a)

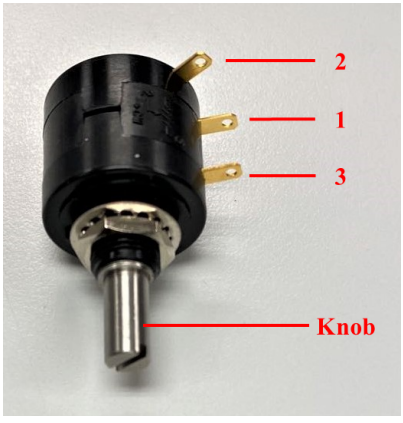


(b)

Figure 4.2: Potentiometer schematic representation.

- ***Modeling***

The rotational potentiometer is used to measure the angular position of the motor and further transmit the corresponding analog value to the microcontroller. As shown in Figure 4.2, terminal 1 and 3 are connected to a resistor element and terminal 2 is connected to an adjustable wiper. Commonly, we have

$$\Omega_{1,3} = \Omega_{1,2} + \Omega_{2,3}. \tag{4.1}$$

where $\Omega_{1,3}$, $\Omega_{1,2}$ and $\Omega_{2,3}$ are the resistance between terminal 1 and 3, terminal 1 and 2 and terminal 2 and 3, respectively. More importantly, $\Omega_{2,3}$ should satisfy the resistance taper [57] as follows:

$$\Omega_{2,3} = k_i\theta. \tag{4.2}$$

where $k$, $i$, $\theta$ denote the taper gradient, the number of potentiometer and the knob position, respectively.

- ***Selection criteria***

To select the proper potentiometers, the resistance taper must be linear and satisfies Equation (4.2). Meanwhile, $k_i$ is computed and expected to be approximately equal to the nominal gradient $k_n$ with linearity tolerance of 0.25% [58]. That is, the taper gradient $k_i$ should satisfy

$$k_i > 0, \tag{4.3}$$

$$k_i \in [99.75\%k_n, 100.25\%k_n]. \tag{4.4}$$

- ***Test procedure***

The resistance taper of the potentiometer is tested as follows. Firstly, we measure the maximum resistance $\Omega_{1,3}$ by putting the probes of ohmmeter on the terminal 1

and 3. Next, we measure the resistance $\Omega_{2,3}$ by taking one of the probes (terminal 3) off and put it on the wiper (terminal 2). Then, we slowly rotate the knob all the way from one end to the other and record the value of $\Omega_{2,3}$ every time the knob rotates 360°. The value should slowly and continually increase with no sudden jumps.

- ***Test results***

The typical results of comparative tests including one control group and three test groups are shown in Table 4.1. It is evident that Groups 1 and 3 fail the test as $k_1, k_3 \notin [2.770, 2.784]$, which is the selective interval computed by the nominal gradient $k_n = 2.777$. Finally, the potentiometer in Group 2 can be selected.

Table 4.1: Taper measurement of the tested potentiometerts.

| Group | 1 | 2 | 3 | Reference |
|---|---|---|---|---|
| $\theta(^\circ)$ | $\Omega_{2,3}$ ($\Omega$) | | | |
| 0 | 0.5 | 0.6 | 0 | 0 |
| 360 | 988 | 1001 | 0 | 1000 |
| 720 | 1982 | 1999 | 0 | 2000 |
| 1080 | 2986 | 2998 | 0 | 3000 |
| 1440 | 3975 | 3998 | 0 | 4000 |
| 1800 | 4970 | 5001 | 0 | 5000 |
| 2160 | 5960 | 6001 | 0 | 6000 |
| 2520 | 6960 | 7000 | 0 | 7000 |
| 2880 | 7950 | 8001 | 0 | 8000 |
| 3240 | 8940 | 9001 | 0 | 9000 |
| 3600 | 9930 | 10001 | 0 | 10000 |
| $k_i(\Omega/^\circ)$ | 2.760 | 2.778 | 0 | 2.777 |

### 4.2.2 Motor Selection

Considering the limitation of resolution and bounded measurement range of the potentiometer, an estimation method is used to select the motors with similar performance. That is, we aim to test the rotational speed for each motor under the same condition by setting the PWM duty cycle at 100% and transmitting the measured data via the same motor interface. The test procedure is shown as follows:

- ***Step 1: Set starting position***

We first set the motor starting position, where is close but not strictly equal to the maximum rotation angle (3600°) of the potentiometer, such that the first sampled data is located in the measurement range with linear taper. Meanwhile, we take 3 test groups for each motor with different starting positions.

- ***Step 2: Compute rotational speed for each test group***

For each test group, the valid data is extracted by discarding the first sampled element. The rotational speed of the $j$th ($j$=1, 2, 3) test group for the $i$th (i=1, 2,...18) motor, denoted by $V_{ij}$, is calculated by the rotation angle per second.

- ***Step 3: Compute average rotational speed for each motor***

Based on the previous step, the average rotation speed of the $i$th motor, denoted by $V_i$, is computed as

$$V_i = \frac{1}{j}\sum_{j=1}^{3} V_{ij} \tag{4.5}$$

- ***Step 4: Select the motors***

We further compute $V_i$ for all the motors and select 12 of those that feature the similar rotational speed, which help reduce the development time. The test results of the computed rotational speed for 18 motors are listed in Table 4.2.

Table 4.2: Test and selection results of 18 motors.

| Motor No. | 1 | 2 | 3 | 4 | 5 | 6 | 7 | 8 | 9 |
|---|---|---|---|---|---|---|---|---|---|
| $V_i(°/s)$ | 615.8 | 675.5 | 412.4 | 512.8 | 692.8 | 667.1 | 649.6 | 628.2 | 656.5 |
| Selection | ✓ | | | | | ✓ | ✓ | ✓ | ✓ |
| Motor No. | 10 | 11 | 12 | 13 | 14 | 15 | 16 | 17 | 18 |
| $V_i(°/s)$ | 645.8 | 629.6 | 705.7 | 614.0 | 654.5 | 636.2 | 588.9 | 634.6 | 673.0 |
| Selection | ✓ | ✓ | | ✓ | ✓ | ✓ | | ✓ | ✓ |

## 4.3 Software Design

### 4.3.1 Firmware Configuration

Firmware is programmed to provide permanent instructions to communicate with other devices and perform basic input/output tasks. It is a packaged program that resides in the microcontroller. To provide a standardized operating environment for the software, the firmware is configured in advance.

In our design, the firmware is configured in STM32CubeMX, which is a graphical configuration and low level code generation tool for STM32 ARM Cortex-M microcontroller. We first select the peripherals to be used by assigning pins to their inputs and outputs. Meanwhile, independent GPIOs are also configured. Next, the system clock is inspected and configured. The "Clock Configuration" tab provides a schematic overview of the clock path, along with the clock sources. After all the embedded software components have been configured and validated, we finally generate the initialization code in C. This code can be used in various development environments, i.e., Keil MDK, GCC, IAR, etc. The pinout and clock configuration are illustrated in Figure 4.3 and 4.4, respectively.

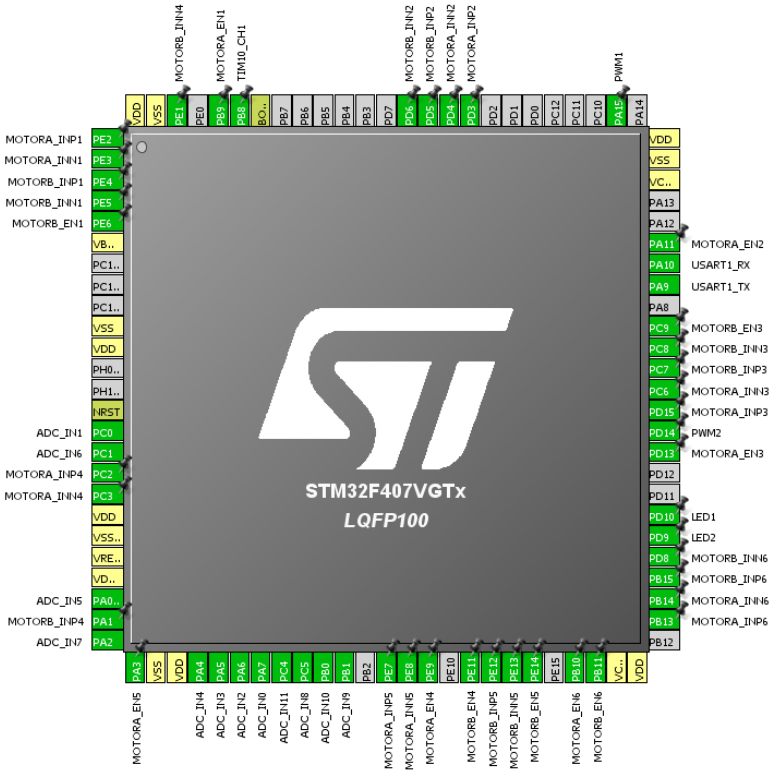


Figure 4.3: Pin configuration of the microcontroller.

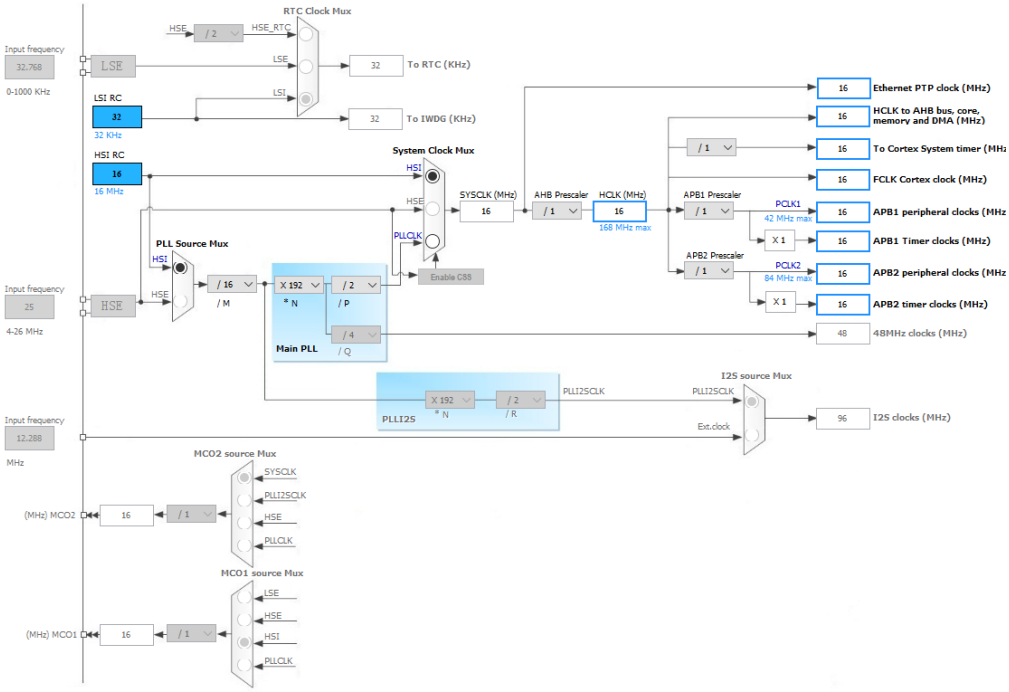


Figure 4.4: Clock configuration of the microcontroller.

### 4.3.2 Software Development

The software is written in C language and runs in Keil MDK. The flowchart of the experimental code is illustrated in Figure 4.5 and the basic descriptions of the functional blocks are provided below.

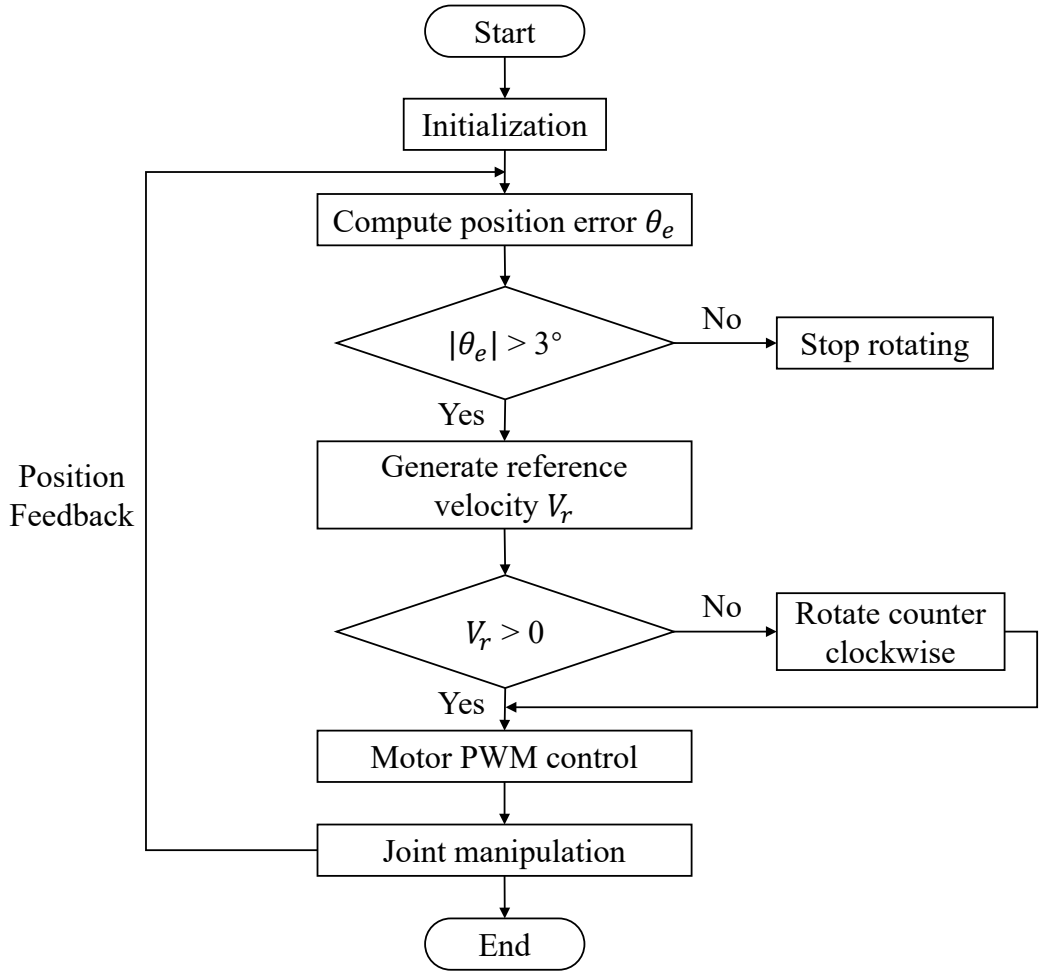


Figure 4.5: Experimental software flowchart.

- ***Step 1: Initialization***

The initial values of the variables used by the software are loaded into registers for fast execution. Moreover, the components, such as pinout, timers, and A/D converters are configured for subsequent control tasks.

- ***Step 2: Compute position error***

Given the desired position $\theta_r$, the analog value of the actual position is measured by the potentiometer and sent to the A/D converter while further converted into the actual position $\theta_a$. The position error $\theta_e$ is calculated as

$$\theta_e = \theta_r - \theta_a. \tag{4.6}$$

- ***Step 3: Generate reference velocity***

The position error $\theta_e$ is then compared with a preset dead zone, specified as 3°. If $\theta_e < 3°$, the motor would brake and stop rotating. Otherwise, the reference velocity $V_r$ is generated by the position controller.

- ***Step 4: Motor PWM control***

The reference velocity serves as the input of the velocity controller to output the corresponding PWM signal, which controls the motor speed and therefore, the angular position $\theta_a$.

- ***Step 5: Joint manipulation***

The robot joints are manipulated by the mounted motors. Meanwhile, the program completes one execution cycle and returns to Step 2.

### 4.3.3 MAF Algorithm Design

The potentiometer rotates at the same angular velocity along with the corresponding motor and outputs the analog signal, which is proportional to the rotation angle. During the experiment, however, measurement errors are existed, therefore, we first test the taper of the potentiometers to eliminate the systematic error coming from the sensors.

Meanwhile, due to relatively low resolution and random noise of the sensors, a moving average filter (MAF) [59] is designed to smooth the array of the sampled data. The filtered digital signal is then converted into the actual joint position $\theta_a$. The designed MAF algorithm is shown below.

**Algorithm 1:** The moving average filtering algorithm

**Define:** *Window[ ]*: An array to store sampled data
*get_adc()*: A function to get sensor value from the A/D converter
**Input:** *sum*: The summation of all the sampled data in one sampling period
*count*: A count variable to be reset after one sampling period
$N$: The number of sampled data in the average
**Output:** *filter_val*

```
1. sum ← 0
2. count ← 0
3. N ← 13
4. if count < N then
       Window[count] ← get_adc()
       sum ← sum + Window[count]
       count ← count + 1
       else
           count ← 0
           filter_val ← (sum/N)
       end
   end
5. Return: filter_val
```

### 4.3.4 Cascaded PID Controller Design

Twelve DC motors are expected to manipulate the joints and thus control the locomotion of the quadruped robot. Hence, a closed-loop joint motion control system is designed using proportional-integral-derivative (PID) strategy. Figure 4.6 illustrates the block diagram of the joint motion system.

In this cascaded control system, the position error $\theta_e$ is first determined between the desired position $\theta_r$ and actual positions $\theta_a$. Passing through the position controller, the reference velocity $V_r$ is then issued as an input to the cascaded velocity

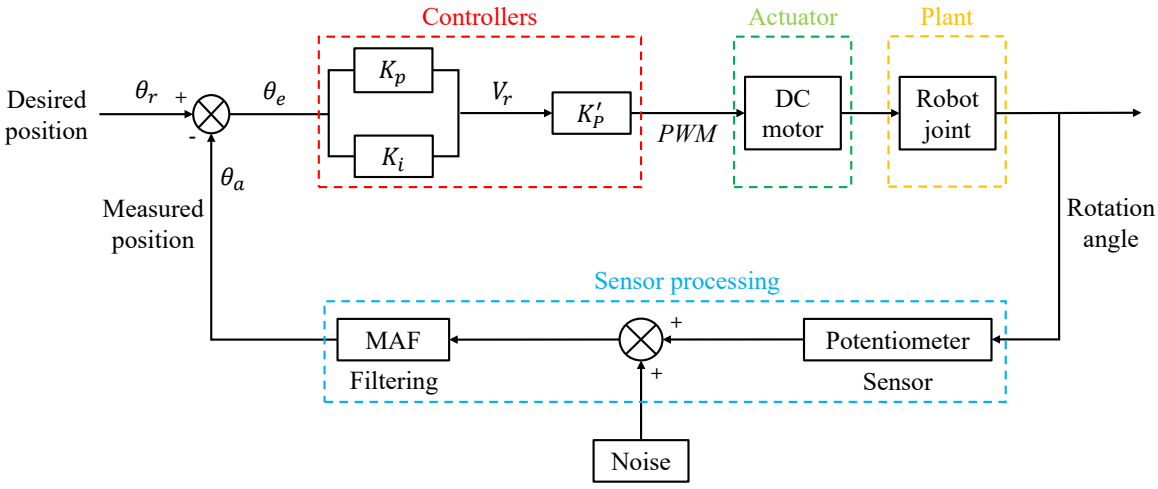


Figure 4.6: Control block diagram of the closed-loop joint motion system.

controller. Scaling by the proportional gain $K_p^{'}$ , the PWM signal is generated to further control the motor speed $V_a$ and the motor position $\theta_a$. In practice, the motor cannot precisely brake and stop at the ideal end position. Therefore, a dead-zone is also set and the motor is expected to stop within a small interval around the target position. In the experiment, the parameters of the controllers and specifications of the joint motion system are listed in Table 4.3.

Table 4.3: Parameter settings of the joint motion control system.

| Index | Value |
|---|---|
| Position controller | $K_p = 0.1, K_i = 0.3, K_d = 0$ |
| Velocity controller | $K_p^{'} = 0.56, K_i^{'} = K_d^{'} = 0$ |
| Sampling frequency (MHZ) | 8 |
| Control frequency (kHZ) | 3.7 |
| Motor dead zone (°) | 3 |

## 4.4 Joint Motion Experiments

### 4.4.1 Knee Joint Test

For convenience, the robot is firstly turned over, as illustrated in Figure 4.7. We aim to manipulate the knee joint into rotating from the actual position $\theta_a = 1980°$ to the desired position $\theta_r = 1780°$. Meanwhile, the angular velocity is required to be decreasing when approaching to the destination. Moreover, the performance of the joints motion in filtered and unfiltered case is tested and the results are shown in Figure 4.8.

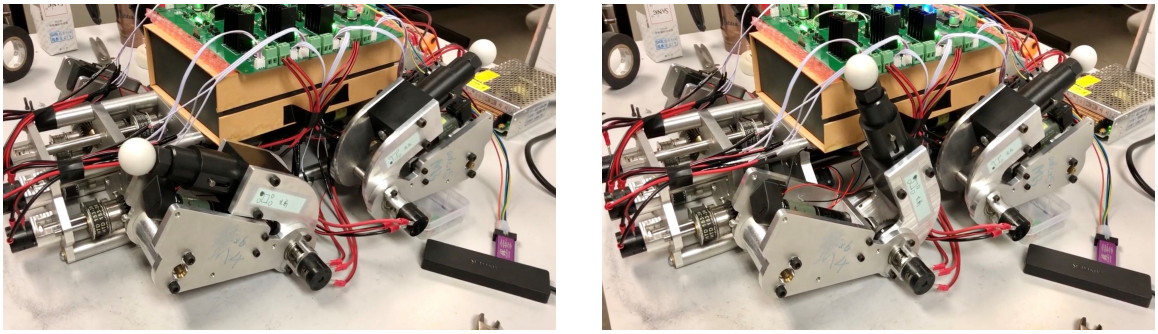

(a) (b)

Figure 4.7: Knee joint rotates from position (a) to (b) in handstand status.

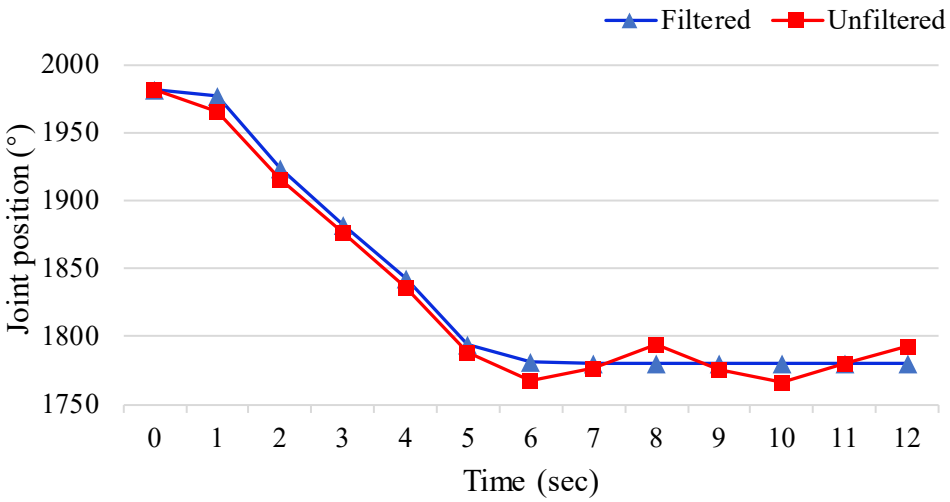


Figure 4.8: Comparison of filtered and unfiltered joint control.

Originally, the objective cannot be achieved when applying the designed control strategy without filtering. As a matter of fact, the motor rotates back and forth around the target position. In addition, the fluctuation range is measured around 26.4°, which is greatly larger than the preset dead-zone, as shown by the red curve. However, after adding the designed MAF and tuning the controller parameters, the joint vibration issue is finally addressed, and all the motor can brake and stop within the preset dead-zone, as illustrated by the blue curve. Thus, the angular position of the knee joint can be controlled.

Next, we recover the robot in standing posture with four legs hanging in the air, and repeat the same test on the knee joint, as pictured in Figure 4.9 (a). The results show that the knee joint can stop at the desired position in Figure 4.9 (b) and verify the feasibility of the proposed joint motion control algorithm.

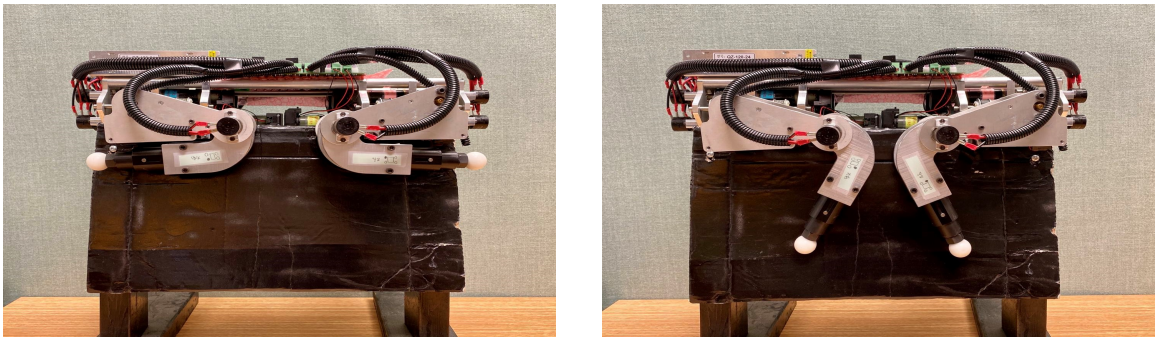

(a) (b)

Figure 4.9: Knee joint rotates from position (a) to (b) in "standing" status.

### 4.4.2 Hip Joint Test

The test of hip joint is not exactly the same as knee joint because of the different mechanical structure and degrees of freedom. Two motors are coupled to be controlled simultaneously, and to complete the motion with cooperation, which increases the complexity of parameter tuning.

In handstand status, the hip joint can somehow reach the set position only if the leg rotates in vertical plane ideally. However, it fails in most cases. The screws used to set the joint mechanical structure become loose when the motor is rotating, and consequently, the torque cannot be transmitted from the motor to the hip joint. In "standing" status, test also fails due to the same reasons. Therefore, the mechanism of the hip joint needs to be further revised or redesigned.

## 4.5 Structural Problems and Solutions in Mechanical Design

During the experiment, the mechanical structure of the hip joint is found unreliable and has negative influence on the motion performance. Moreover, solutions are required to eliminate the problems of loose screws.

- ***Motor and brass shaft***

A screw assembled to fix the motor shaft and brass shaft will loose when rotating. As a result, the torque cannot be transmitted from the motor to the brass shaft. Instead of screw fixation, the keyed joint structure [60] is preferable, which can effectively protect the motor shaft, and meanwhile extend its service life.

- ***Bevel gear and pulley***

Similarly, the screws used to fix bevel gear 1 and pulley 2 on the shaft sleeve are always loose, which leads to asynchronous rotation between these two components. To solve this, a keyway is firstly machined on the shaft sleeve and a proper standard key is then selected. The keyed joint restricts the relative rotational movement between the shaft and rotation element, and guarantees torque transmission. The same structural solution is applicable to the bevel gear 2 and pulley 3, as illustrated in Figure 4.10.

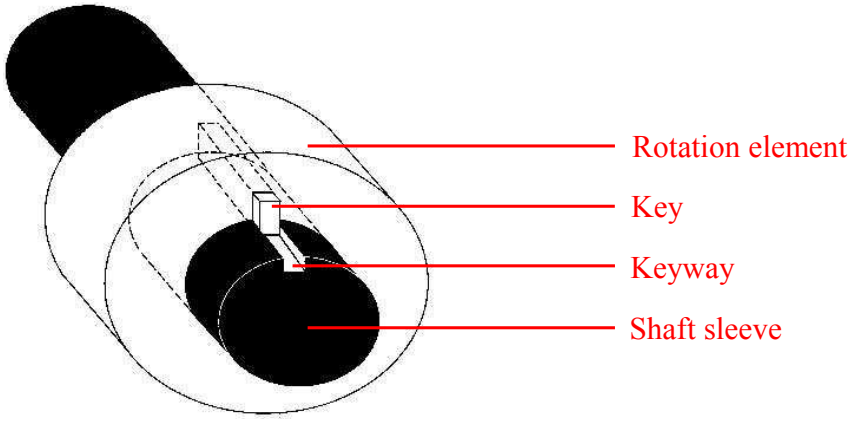


Figure 4.10: Keyed joint connection between bevel gear and shaft sleeve.

## 4.6 Conclusions

Software and hardware are indispensable parts to set up the experiment platform. In our design, the hardware including motors and sensors is firstly tested and picked out for the experiment. In addition, firmware is configured in STM32CubeMX and software is then developed specifically for motor control.

Next, a closed-loop joint motion control system is presented. The cascaded PID control law is designed and is implemented to control the position and velocity of the motors. To reduce random noise, the MAF is also designed for sensor processing.

In addition, the joint motion experiments are conducted. The results show that the knee joint is able to rotate at different speed and finally stop at the desired position. Meanwhile, feasibility of the designed joint motion control algorithm is verified.

# Chapter 5

# Conclusions and Future Work

## 5.1 Conclusions

In this thesis, the embedded system design and joint motion control of a quadruped robot have been presented.

The overall structures and specifications of the quadruped robot have been introduced in **Chapter 2**. By analyzing the joint structures, the motion mechanism of the robot legs and two walking patterns have been illustrated. Moreover, the detailed development procedures of this project have been discussed.

The embedded system hardware design of the quadruped robot has been presented in **Chapter 3**. According to the functional requirements and marketing research, the onboard components of the embedded system have been selected. By illustrating the hardware architecture, the circuit schematic diagrams for all functional modules have been introduced. The PCB information and comparison of two versions design have been provided.

The MAF-based cascaded PID control strategy for dealing with the robot joint motion system has been proposed in **Chapter 4**. With the combination of hardware

testing, firmware configuration, and software development, the robot experimental platform has been setup. To control the motor position and velocity, cascaded PID controllers have been designed and implemented on two types of joints. In addition, the moving average filter has been added to reduce the noise and obtain reliable sampled data. Finally, the experimental tests have been conducted to verify the effectiveness of the proposed control algorithm.

## 5.2 Future Work

The results of this work open a variety of interesting areas and the quadruped robot can be further developed from the following aspects.

- ***Improvement of the robot leg structure***

The existing leg structure can be redesigned to effectively transmit the actuator torque to the operational joints. Two DOFs of the hip joint can be designed separately to decrease the difficulty of assembly and control strategy implementation. Moreover, an additional passive ankle joint is considered for rough terrain mobility, as shown in Figure 5.1.

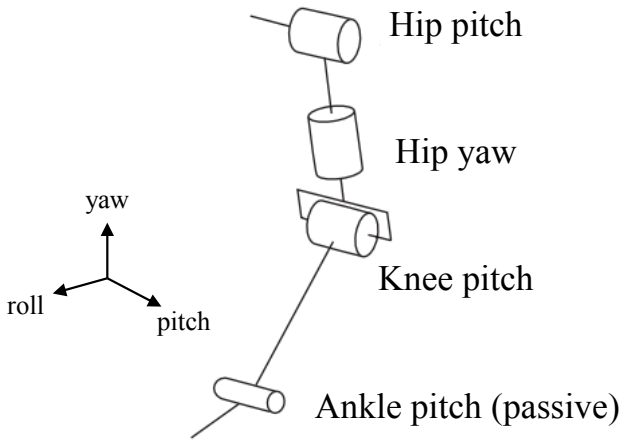


Figure 5.1: Leg structure with three active joints and one passive joint [61].

- ***Selection of actuator and sensor***

The actuators and sensors can be more appropriately selected. The motor with high reduction ratio can be utilized not only to enlarge the output torque, but also to reduce the moment of inertia for quick motion and response. To increase environment perception of the robot, different types of sensors can be used to complete certain tasks.

- ***Hierarchical network communication***

Similar to the PCB structure, the robotic control consists of different layers, which contain either singular or multiple parallel processes. By using hybrid control [62], the robot behavior can be governed. Typically, the structure of hybrid control includes low level, mid level, and high level.

To further control the robot locomotion, we should develop the hierarchical structure of the robot, and embed it in the practical control system. The online vision-based system can be applied to conduct image processing using FPGA. Based on the feedback data, local maps and walking patterns are generated by the high-level controller. Additionally, the torque and position commands will be sent to the motor for further control on the joint motion and robot locomotion.

# Bibliography

[1] G. Piras, W. L. Cleghorn, and J. K. Mills, "Dynamic finite-element analysis of a planar high-speed, high-precision parallel manipulator with flexible links," *Mechanism and Machine Theory*, vol. 40, no. 7, pp. 849–862, Jul. 2005.

[2] Z. Li, Z. Huang, and Y. Huang, "Design of spot welding robot," *TELKOMNIKA Indonesian Journal of Electrical Engineering*, vol. 11, no. 11, pp. 6267–6273, Nov. 2013.

[3] S. Kudoh, K. Ogawara, M. Ruchanurucks, and K. Ikeuchi, "Painting robot with multi-fingered hands and stereo vision," *Robotics and Autonomous Systems*, vol. 57, no. 3, pp. 279–288, Mar. 2009.

[4] P. McGuire, J. Fritsch, J. J. Steil, F. Rothling, G. A. Fink, S. Wachsmuth, G. Sagerer, and H. Ritter, "Multi-modal human-machine communication for instructing robot grasping tasks," in *Proceedings of IEEE/RSJ International Conference on Intelligent Robots and Systems*, vol. 2, pp. 1082–1088, Aug. 2002.

[5] A. Bechar and C. Vigneault, "Agricultural robots for field operations. Part 2: Operations and systems," *Biosystems Engineering*, vol. 153, pp. 110–128, Jan. 2017.

[6] M. Takahashi, T. Suzuki, H. Shitamoto, T. Moriguchi, and K. Yoshida, "Developing a mobile robot for transport applications in the hospital domain," *Robotics and Autonomous Systems*, vol. 58, no. 7, pp. 889–899, Jul. 2010.

[7] C. Wang and D. Du, "Research on logistics autonomous mobile robot system," in *Proceedings of IEEE International Conference on Mechatronics and Automation*, pp. 275–280, Aug. 2016.

[8] C. H. Lee, S. H. Kim, S. C. Kang, M. S. Kim, and Y. K. Kwak, "Double-track mobile robot for hazardous environment applications," *Advanced Robotics*, vol. 17, no. 5, pp. 447–459, Jan. 2003.

[9] A. Preumont, P. Alexandre, I. Doroftei and F. Goffin, "A conceptual walking vehicle for planetary exploration," *Mechatronics*, vol. 7, no. 3, pp. 287–296, Apr. 1997.

[10] P. Fiorini, "Ground mobility systems for planetary exploration," in *Proceedings of IEEE International Conference on Robotics and Automation*, vol. 1, pp. 908-913, Apr. 2000.

[11] T. Huntsberger, A. Stroupe, and B. Kennedy, "System of systems for space construction," in *Proceedings of IEEE International Conference on Systems, Man and Cybernetics*, vol. 4, pp. 3173–3178, Oct. 2005.

[12] H. Hasunuma, K. Nakashima, M. Kobayashi, F. Mifune, Y. Yanagihara, T. Ueno, K. Ohya, and K. Yokoi, "A tele-operated humanoid robot drives a backhoe," in *Proceedings of IEEE International Conference on Robotics and Automation*, vol. 3, pp. 2998–3004, Sep. 2003.

[13] M. A. Armada, M. Tavakoli, M. R. Zakerzadeh, G. R. Vossoughi, and S. Bagheri, "A hybrid pole climbing and manipulating robot with minimum DOFs for construction and service applications," *Industrial Robot: An International Journal*, vol. 32, pp. 171–178, Apr. 2005.

[14] Y. Mae, A. Yoshida, T. Arai, K. Inoue, K. Miyawaki, and H. Adachi, "Application of locomotive robot to rescue tasks," in *Proceedings of IEEE International Conference on Intelligent Robots and Systems*, vol. 3, pp. 2083–2088, Nov. 2000.

[15] Y. Iwano, K. Osuka and H. Amano, "Development of stretcher component robots for rescue activity," in *Proceedings of IEEE International Conference on Robotics, Automation and Mechatronics*, vol. 2, pp. 915–920, Dec. 2004.

[16] Y. Ogura, H. Aikawa, K. Shimomura, H. Kondo, A. Morishima, H. O. Lim, and A. Takanishi, "Development of a new humanoid robot WABIAN-2," in *Proceedings of IEEE International Conference on Robotics and Automation*, pp. 76–81, May. 2006.

[17] H. Lim, Y. Sugahara, and A. Takanishi, "Development of a biped locomotor applicable to medical and welfare fields," in *Proceedings of IEEE/ASME International Conference on Advanced Intelligent Mechatronics*, pp. 950–955, Jul. 2003.

[18] J. M. Conrad, "Stiquito for robotics and embedded systems education," *Computer*, vol. 38, no. 6, pp. 77–81, Jun. 2005.

[19] Y. J. Lee, and S. Hirose, "Three-legged walking for fault tolerant locomotion of a quadruped robot with demining mission," in *Proceedings of IEEE/RSJ International Conference on Intelligent Robots and Systems*, vol. 2, pp. 973–978, Oct. 2000.

[20] D. Spenneberg, K. McCullough, and F. Kirchner, "Stability of walking in a multi-legged robot suffering leg loss," in *Proceedings of IEEE International Conference on Robotics and Automation*, vol. 3, pp. 2159–2164, Apr. 2004.

[21] P. G. Santos, J. A. Gálvez, J. Estremera, and E. Garcia, "SIL04: A true walking robot for the comparative study of walking machine techniques," *IEEE Robotics and Automation Magazine*, vol. 10, no. 4, pp. 23–32, Dec. 2003.

[22] R. Tajima and K. Suga, "Motion having a flight phase: Experiments involving a one-legged robot," in *Proceedings of IEEE/RSJ International Conference on Intelligent Robots and Systems*, pp. 1726–1731, Oct. 2006.

[23] D. W. Haldane, J. K. Yim, and R. S. Fearing, "Repetitive extreme-acceleration (14-g) spatial jumping with Salto-1P," in *Proceedings of IEEE/RSJ International Conference on Intelligent Robots and Systems*, pp. 3345–3351, Sep. 2017.

[24] J. K. Yim , E. K. Wang, and R. S. Fearing, "Drift-free roll and pitch estimation for high-acceleration hopping," in *Proceedings of IEEE International Conference on Robotics and Automation*, pp. 8986–8992, May. 2019.

[25] Reem-C Technical Specifications [Online].
Avaliable: http://pal-robotics.com/robots/reem-c

[26] O. Stasse, T. Flayols, R. Budhiraja, K. Giraud-Esclasse, J. Carpentier, J. Mirabel, A. Del Prete, P. Souères, N. Mansard, F. Lamiraux, and J. P. Laumond, "TALOS: A new humanoid research platform targeted for industrial applications," in *Proceedings of IEEE-RAS International Conference on Humanoid Robotics*, pp. 689–695, Nov. 2017.

[27] C. Semini, V. Barasuol, M. Focchi, C. Boelens, M. Emara, S. Casella, O. Villarreal, R. Orsolino, G. Fink, S. Fahmi, G. Medrano-Cerda, and D. G. Caldwell,

"Brief introduction to the quadruped robot hyqreal," in *Istituto di Robotica e Macchine Intelligenti (I-RIM)*, 2019.

[28] G. Bledt, M. J. Powell, B. Katz, J. Di Carlo, P. M. Wensing, and S. Kim, "MIT Cheetah 3: Design and control of a robust, dynamic quadruped robot," in *Proceedings of IEEE/RSJ International Conference on Intelligent Robots and Systems*, pp. 2245–2252, Oct. 2018.

[29] Unitree Laikago [Online]. Avaliable: http://www.unitree.cc

[30] M. Hutter, C. Gehring, D. Jud, A. Lauber, C. D. Bellicoso, V. Tsounis, J. Hwangbo, K. Bodie, P. Fankhauser, M. Bloesch, and R. Diethelm, "Anymal-a highly mobile and dynamic quadrupedal robot," in *Proceedings of IEEE/RSJ International Conference on Intelligent Robots and Systems*, pp. 38–44, Oct. 2016.

[31] P. Ben-Tzvi, A. A. Goldenberg, and J. W. Zu, "Design, simulations and optimization of a tracked mobile robot manipulator with hybrid locomotion and manipulation capabilities," in *Proceedings of IEEE International Conference on Robotics and Automation*, pp. 2307–2312, May. 2008.

[32] M. Simi, P. Valdastri, C. Quaglia, A. Menciassi, and P. Dario, "Design, fabrication, and testing of a capsule with hybrid locomotion for gastrointestinal tract exploration," *IEEE/ASME Transactions on Mechatronics*, vol. 15, no. 2, pp. 170–180, Feb. 2010.

[33] M. Schwarz, T. Rodehutskors, M. Schreiber, and S. Behnke, "Hybrid driving-stepping locomotion with the wheeled-legged robot Momaro," in *Proceedings of IEEE International Conference on Robotics and Automation*, pp. 5589–5595, May. 2016.

[34] N. G. Tsagarakis, G. Metta, G. Sandini, D. Vernon, R. Beira, F. Becchi, L. Righetti, J. Santos-Victor, A. J. Ijspeert, M. C. Carrozza, and D. G. Caldwell, "iCub: The design and realization of an open humanoid platform for cognitive and neuroscience research," *Advanced Robotics*, vol. 21, no. 10, pp. 1151–1175, Jan. 2007.

[35] A. Kroll, W. Baetz, and D. Peretzki, "On autonomous detection of pressured air and gas leaks using passive IR-thermography for mobile robot application," in *Proceedings of IEEE International Conference on Robotics and Automation*, pp. 921–926, May. 2009.

[36] Y. Tanaka, S. Sakama, K. Nakano, H. Kosodo, "Comparative study on dynamic characteristics of hydraulic, pneumatic and electric motors," in *ASME/BATH Symposium on Fluid Power and Motion Control*, Oct. 2013.

[37] J. S. Chiang, C. H. Hsia, S. H. Chang, W. H. Chang, H. W. Hsu, Y. C. Tai, C. Y. Li, and M. H. Ho, "An efficient object recognition and self-localization system for humanoid soccer robot," in *Proceedings of SICE Annual Conference*, pp. 2269–2278, Aug. 2010.

[38] D. F. Wolf and G. S. Sukhatme, "Semantic mapping using mobile robots," *IEEE Transactions on Robotics*, vol. 24, no. 2, pp. 245–258, Apr. 2008.

[39] J. P. Cruz, M. L. Dimaala, L. G. Francisco, E. J. Franco, A. A. Bandala, and E. P. Dadios, "Object recognition and detection by shape and color pattern recognition utilizing Artificial Neural Networks," in *Proceedings of IEEE International Conference of Information and Communication Technology*, pp. 140–144, Mar. 2013.

[40] J. G. Velásquez-Aguilar, M. Granados-Contreras, A. Ramirez-Agundis, and F. Aquino-Roblero, "Hybrid object detection vision-based applied on mobile robot navigation," in *Proceedings of IEEE International Conference on Mechatronics, Electronics and Automotive Engineering*, pp. 51–56, Nov. 2015.

[41] Embedded system & robotics [Online].
Avaliable: https://www.slideshare.net/rynraj27/embedded-system-robotics

[42] K. Berns, W. Ilg, M. Deck, J. Albiez, and R. Dillmann, "Mechanical construction and computer architecture of the four-legged walking machine BISAM," *IEEE/ASME Transactions on Mechatronics*, vol. 4, no. 1, pp. 32–38, Mar. 1999.

[43] H. Kimura, Y. Fukuoka, and H. Katabuti, "Mechanical design of a quadruped "Tekken3&4"and navigation system using laser range sensor," in *International Symposium on Robotics*, vol. 36, no. 1, Nov. 2005.

[44] Altium: PCB Design Software and Tools [Online].
Avaliable: https://www.altium.com

[45] 10 Steps to Selecting a Microcontroller [Online]. Avaliable:
https://community.arm.com/developer/ip-products/system/b/embedded-blog/posts/10-steps-to-selecting-a-microcontroller

[46] 2017 Embedded Markets Study [Online].
Avaliable: https://m.eet.com/media/1246048/2017-embedded-market-study.pdf

[47] Robot operating system [Online]. Avaliable: https://www.ros.org

[48] J. Caxias, F. A. Silva, J. Sequeira, "Transmission line inspection robots: Design of the power supply system," in *Proceedings of IEEE International Conference on Applied Robotics for the Power Industry*, pp. 1–6, Oct. 2010.

[49] J. H. Lever, A. Streeter, and L. R. Ray, "Performance of a solar-powered robot for polar instrument networks," in *Proceedings of IEEE International Conference on Robotics and Automation*, pp. 4252–4257, May. 2006.

[50] F. Caricchi, F. Crescimbini, F. Capponi, and L. Solero, "Study of bi-directional buck-boost converter topologies for application in electrical vehicle motor drives," in *APEC'98 Thirteenth Annual Applied Power Electronics Conference and Exposition*, vol. 1, pp. 287–293, Feb. 1998.

[51] D. Peng, J. Zhang, and L. Wang, "Experimental result on wireless power management microsystem for endoscopic capsule robot," in *Proceedings of IEEE-EMBS International Conference on Biomedical and Health Informatics*, pp. 810–813, Jan. 2012.

[52] STM32F405xx/407xx data sheet - production data [Online].
Avaliable: https://www.st.com/resource/en/datasheet/stm32f405rg.pdf

[53] V. D. Blank, V. S. Bormashov, S. A. Tarelkin, S. G. Buga, M. S. Kuznetsov, D. V. Teteruk, N. V. Kornilov, S. A. Terentiev, and A. P. Volkov, "Power high-voltage and fast response Schottky barrier diamond diodes," *Diamond and Related Materials*, vol. 57, pp. 32–36, Aug. 2015.

[54] S. Muralikrishna and S. Sathyamurthy, "An overview of digital circuit design and PCB design guidelines - An EMC perspective," in *Proceedings of IEEE International Conference on Electromagnetic Interference & Compatibility*, pp. 567–573, Nov. 2008.

[55] M. R. Islam and T. A. Rahman, "Novel and simple design of multi layer radial line slot array (RLSA) antenna using FR-4 substrate," in *Proceedings of IEEE*

*International Conference on Electromagnetic Compatibility*, pp. 843–846, May. 2008.

[56] M. Shinagawa, J. Katsuyama, K. Matsumoto, S. Hasegawa, R. Sugiyama, and Y. Kado, "Noise analysis for intra-body communication based on parasitic capacitance measurement," *Measurement*, vol. 51, pp. 206–213, May. 2014.

[57] Potentiometer taper [Online].
Avaliable: http://www.resistorguide.com/potentiometer-taper

[58] Independent linearity tolerance [Online].
Avaliable: http://sakae-tsushin.co.jp/eng_page/pdf/pot/e_22HP.pdf

[59] S. Golestan, M. Ramezani, J. M. Guerrero, F. D. Freijedo, and M. Monfared, "Moving average filter based phase-locked loops: Performance analysis and design guidelines," *IEEE Transactions on Power Electronics*, vol. 29, no. 6, pp. 2750–2763, Jul. 2013.

[60] D. Zanotto, P. Stegall, S. K. Agrawal, "ALEX III: A novel robotic platform with 12 DOFs for human gait training," in *Proceedings of IEEE International Conference on Robotics and Automation*, pp. 3914–3919, May. 2013.

[61] H. Kimura, Y. Fukuoka, and A. H. Cohen, "Adaptive dynamic walking of a quadruped robot on natural ground based on biological concepts," *The International Journal of Robotics Research*, vol. 26, no. 5, pp. 475–490, May. 2007.

[62] J. Malmborg, "Analysis and Design of Hybrid Control Systems," *Department of Automatic Control Lund Institute of Technology, Sweden*, May. 1998.